

# EVOLUTION OF THE SOLAR ACTIVITY OVER TIME AND EFFECTS ON PLANETARY ATMOSPHERES: I. HIGH-ENERGY IRRADIANCES (1–1700 Å)

IGNASI RIBAS<sup>1</sup>, EDWARD F. GUINAN<sup>2</sup>, MANUEL GÜDEL<sup>3</sup>, AND MARC AUDARD<sup>4</sup>

*Submitted to ApJ*

## ABSTRACT

We report on the results of the Sun in Time multi-wavelength program (X-rays to the UV) of solar analogs with ages covering  $\sim$ 0.1–7 Gyr. The chief science goals are to study the solar magnetic dynamo and to determine the radiative and magnetic properties of the Sun during its evolution across the main sequence. The present paper focuses on the latter goal, which has the ultimate purpose of providing the spectral irradiance evolution of solar-type stars to be used in the study and modeling of planetary atmospheres. The results from the Sun in Time program suggest that the coronal X-ray–EUV emissions of the young main-sequence Sun were  $\sim$ 100–1000 times stronger than those of the present Sun. Similarly, the transition region and chromospheric FUV–UV emissions of the young Sun are expected to be 20–60 and 10–20 times stronger, respectively, than at present. When considering the integrated high-energy emission from 1 to 1200 Å the resulting relationship indicates that the solar high-energy flux was about 2.5 times the present value 2.5 Gyr ago and about 6 times the present value about 3.5 Gyr ago (when life supposedly arose on Earth). The strong radiation emissions inferred should have had major influences on the thermal structure, photochemistry, and photoionization of planetary atmospheres and also played an important role in the development of primitive life in the Solar System. Some examples of the application of the Sun in Time results on exoplanets and on early Solar System planets are discussed.

*Subject headings:* stars: late-type — stars: chromospheres — stars: coronae — stars: activity — Sun: evolution — solar-terrestrial relations

## 1. INTRODUCTION

The Sun is by far the most important star to us. Without a dependable (stable) star like the Sun, the Earth would not have developed a rich and diverse biosphere that is home to millions of species of life. Because of ever accelerating nuclear reactions in its core, the Sun is a slowly evolving variable star that has undergone a  $\sim$ 40% increase in luminosity over the last 4.5 Gyr, as predicted by the standard solar evolution model (e.g., Girardi et al. 2000). On much shorter timescales, we know that the Sun is also a magnetic variable star, with an  $\sim$ 11-yr sunspot and activity cycle and a  $\sim$ 22-yr magnetic cycle. As predicted by magnetic dynamo theory, the Sun’s rotation ( $P_{\text{rot}} \sim 25.5$  d) and convective outer envelope interact to generate magnetic fields (Parker 1970). The magnetic dynamo-generated energy is released in the form of flares and chromospheric, transition-region, and coronal radiation. Satellite observations of the Sun show that it undergoes small (0.10–0.15%) variations in total brightness over its activity cycle, although the changes at short wavelengths (UV to X-rays) are much more pronounced (10–500%) (Lean 1997).

The magnetic activity of the present Sun is feeble relative to other solar-type stars, but magnetic-induced phenomena still have important effects on Earth and the Solar System (see Guinan & Ribas 2002). Thus, the fundamental question whether the Sun has always been a relatively inactive star or if, in contrast, it has experienced some periods of stronger magnetic activity has a strong impact on the evolution of the Solar System. Compelling observational evidence (Güdel et al. 1997a) shows that zero-age main sequence (ZAMS) solar-type

stars rotate over 10 times faster than today’s Sun. As a consequence of this, young solar-type stars, including the young Sun, have vigorous magnetic dynamos and correspondingly strong high-energy emissions. From the study of solar type stars with different ages, Skumanich (1972), Simon et al. (1985), and others showed that the Sun loses angular momentum with time via magnetized winds (magnetic braking) thus leading to a secular increase of its rotation period (Durney 1972). This rotation slow-down is well fitted by a power law roughly proportional to  $t^{-1/2}$  (e.g., Skumanich 1972; Soderblom 1981; Ayres 1997). Note that the age–rotation period relationship is tighter for intermediate/old stars, while young stars (a few  $10^8$  yr) show a larger spread in rotation periods. In response to slower rotation, the solar dynamo strength diminishes with time causing the Sun’s high-energy emissions also to undergo significant decreases. Comprehensive studies on this subject were published by Zahnle & Walker (1982) and Ayres (1997). The reader is referred to these publications for background information on solar-type stars’ upper atmospheres and related high-energy emissions.

The “Sun in Time” program was established some 20 years ago (Dorren & Guinan 1994; Guinan & Ribas 2004) to study a sample of accurately-selected solar proxies (G0–G5 V stars) with different ages across the electromagnetic spectrum. The primary aims of the program are: 1) To test dynamo models of the Sun in which rotation is the only significant variable parameter, and 2) to determine the spectral irradiance of the Sun over its main-sequence lifetime. In the present paper, we focus on the latter goal, which has the ultimate purpose of characterizing the evolution of the solar emissions with direct application to

<sup>1</sup>Institut d’Estudis Espacials de Catalunya/CSIC, Campus UAB, Facultat de Ciències, Torre C5 - parell - 2a planta, 08193 Bellaterra, Spain; E-mail: [ribas@ieec.uab.es](mailto:ribas@ieec.uab.es)

<sup>2</sup>Department of Astronomy & Astrophysics, Villanova University, Villanova, PA 19085, USA; E-mail: [edward.guinan@villanova.edu](mailto:edward.guinan@villanova.edu)

<sup>3</sup>Paul Scherrer Institut, Würenlingen & Villigen, 5232 Villigen PSI, Switzerland; E-mail: [guedel@astro.phys.ethz.ch](mailto:guedel@astro.phys.ethz.ch)

<sup>4</sup>Columbia Astrophysics Laboratory, Columbia University, 550 West 120th Street, New York, NY 10027, USA; E-mail: [audard@astro.columbia.edu](mailto:audard@astro.columbia.edu)

the study and modeling of atmospheres of both Solar System planets and exoplanets in orbit around solar-type stars. There are a number of aspects within the Solar System in which a stronger high-energy flux from the young Sun could have had a critical impact. Through photochemical and photoionization processes, the strong X-ray and UV emissions of the young Sun could have had a major effect on the evolution of the atmospheres, ionospheres and climates of the terrestrial planets, including the Earth (e.g., Canuto et al. 1982, 1983; Kasting & Catling 2003; Smith et al. 2004). For example, paleo-climate models of the Earth should account for the higher levels of ionizing and dissociating UV radiation in the past. Even the development of life on Earth (and possibly on Mars) could have been influenced by the larger doses of sterilizing UV radiation expected from the young Sun (cf. Cockell et al. 2000).

In this paper we present the results of an investigation on the long-term magnetic history of the Sun, focused on the high-energy emissions (below 1700 Å). Basically, we study the chromospheric, transition region and coronal emissions, associated to high-temperature atmospheric layers. In contrast, the time evolution of the photospheric emissions is already well characterized because these scale with the overall bolometric luminosity. We have made use of our selected sample of stellar proxies with ages that cover most of the main-sequence lifetime of the Sun. A large number of multiwavelength observations (X-ray, EUV, FUV, UV; hereafter XUV) of the solar analogs have been collected to fully describe their spectral irradiances as a function of age and rotation. Also discussed are the major effects that the young Sun's strong XUV radiation may have had on the photoionization, photochemistry, and erosion of paleo-planetary atmospheres.

## 2. THE SUN IN TIME SAMPLE

A critical element to any study of the evolution of the Sun's irradiance with time is a carefully-selected sample of stars to serve as proxies for the Sun with different rotation periods, and therefore different ages. The Sun in Time sample contains single or widely separated binary, nearby, G0–5 stars that have known rotation periods and well-determined temperatures, luminosities, and metallicities. In addition, we have been able to estimate the stellar ages by making use of their memberships in clusters and moving groups, rotation period–age relationships, and, for the older stars, fits to stellar evolution models. Comparisons with stellar models predict stellar masses within 10% of  $1 M_{\odot}$ . While the complete Sun in Time sample contains over 15 solar analogs, we focus here on six stars that have been observed with a variety of high-energy instruments: EK Dra,  $\pi^1$  UMa,  $\chi^1$  Ori,  $\kappa^1$  Cet,  $\beta$  Com, and  $\beta$  Hyi. These solar analogs cover most of the Sun's main sequence lifetime at approximate ages of 100 Myr, 300 Myr, 650 Myr, 1.6 Gyr, and 6.7 Gyr. Note that we have not used any proxy for the current Sun but the Sun itself. Although there are no full-disk high-resolution spectra of the Sun (as pointed out by Pagano et al. 2004), the datasets described in §3.5 have sufficient resolution to fulfill the requirements of the present study. If higher resolution data were necessary, a valid alternative would be to use solar twins. For example, 18 Sco is a nearly perfect solar twin (Porto de Mello & da Silva 1997; Hamilton et al. 2003), but few high-energy observations are available because of its relative faintness.  $\alpha$  Cen A is slightly more massive than the Sun but yet a good solar twin (Pagano et al. 2004) and with numerous observations. In this case, however, some of the high-energy observations include the emissions from the active K-type companion  $\alpha$  Cen

B, which complicates the analysis significantly.

A discussion of each observed target is provided below and a summary of the relevant stellar data (including those for the Sun) is shown in Table 1. Stellar radii have been estimated from the observed magnitude, distance, and temperature, while masses generally follow from evolutionary model calculations. Also given in Table 1 is the estimated value of the solar radius at the corresponding age as provided by the stellar models of Girardi et al. (2000).

**EK Dra:** This is a nearby G1.5 V star that has traditionally been considered among the most active solar analogs in our neighborhood. Its main properties were reviewed by Strassmeier & Rice (1998) and Messina & Guinan (2003), including an average rotation period of 2.68 days. Evolutionary models of Girardi et al. (2000) yield a slightly super-solar mass and a ZAMS age at the observed temperature, luminosity and chemical composition (solar) of EK Dra. Montes et al. (2001a,b), and references therein, classified EK Dra as a kinematic member of the so-called Local Association or Pleiades moving group (with an estimated age range of 20–150 Myr) but inferred an age younger than the Pleiades cluster from the observed Li abundance. Similar conclusions were drawn by Wichmann et al. (2003), who obtained an upper limit to the age of EK Dra of 50–100 Myr. Here we adopt an age of  $\sim$ 100 Myr, which seems to be a good compromise. Note that EK Dra was found to be a radial velocity variable by Duquennoy & Mayor (1991) with a period of about 12.5 yr. This companion to EK Dra would have a minimum mass below  $0.4 M_{\odot}$  and thus likely be an M-type star. Metchev & Hillenbrand (2004) have recently reported the discovery of a companion to EK Dra with a mass of  $0.20^{+0.30}_{-0.08} M_{\odot}$  using adaptive optics. It is not yet clear whether these two low-mass companions detected independently are indeed the same. In any case, neither of them is a concern for our studies since they should only contribute a few percent in the wavelength domain of interest.

**$\pi^1$  UMa:** This young solar proxy is an active G1.5 V star with a rotation period of about 4.9 days (Messina & Guinan 2003). Gaidos & González (2002) and Ottmann et al. (1998) carried out detailed spectroscopic analyses and determined accurate values for the stellar temperature and metal abundance (compatible with solar). Evolutionary models of Girardi et al. (2000) indicate a mass just a few percent higher than that of the Sun. Kinematic studies such as those of Montes et al. (2001a,b) and King et al. (2003) classify  $\pi^1$  UMa as a probable member of the Ursa Major moving group. Although the age of this kinematic group of stars has traditionally been quoted as about 300 Myr (see, e.g., Soderblom & Mayor 1993), recent work by King et al. (2003) suggests an older age of  $500 \pm 100$  Myr on the basis of a number of complementary criteria. Here we prefer to adopt the canonical age of  $\sim$ 300 Myr since it stands in much better agreement with our measured high-energy fluxes as discussed below.

**$\chi^1$  Ori:** This field G1 V star has a rotation period of about 5.2 days (Messina et al. 2001), which is indicative of its young age. Its temperature and metal abundance (slightly sub-solar) were determined by Gratton et al. (1998) and Taylor (2003a,b) with very similar results. King et al. (2003) classified  $\chi^1$  Ori as a certain member of the Ursa Major moving group in agreement with a number of previous studies. In accordance with  $\pi^1$  UMa, we have adopted an age estimate of  $\sim$ 300 Myr. Interestingly,  $\chi^1$  Ori is a spectroscopic binary with an orbital period of about 14 yr (Han & Gatewood 2002) that was recently resolved using adaptive optics at Keck by König et al. (2002). These authors

were able to determine the dynamical mass of both  $\chi^1$  Ori and its companion. Note that, with a mass of only  $0.15 M_{\odot}$ , the quiescent high-energy emissions of  $\chi^1$  Ori B will be negligibly small compared to those of its much larger primary companion.

**$\kappa^1$  Cet:** With spectral type G5 V, this star the coolest in the sample. Spectroscopic parameters were determined by Gaidos & González (2002), who also estimated slightly super-solar metal content. Its rotation period was reported to be around 9.2 days by Messina & Guinan (2003), in agreement with other determinations. Evolutionary models of Girardi et al. (2000) yield a mass very close to the solar value. In the kinematic study of Montes et al. (2001a)  $\kappa^1$  Cet was not flagged as a member of any of the canonical stellar groups but was classified as a young disk star. In the absence of more direct indicators, we estimate the age of  $\kappa^1$  Cet from its rotation period and mean X-ray luminosity ( $\log L_X = 28.8$  [erg s $^{-1}$ ]; Güdel et al. 1997a). Comparison with Hyades stars in the same (B-V) interval as  $\kappa^1$  Cet reveals that both its rotation period (cf. Radick et al. 1995) and its X-ray luminosity (cf. Barrado y Navascués et al. 1998) are close to the average of the Hyades members. These criteria suggest for  $\kappa^1$  Cet an age close to the canonical Hyades age of  $\sim 650$  Myr, which we subsequently adopt. Note that our value is older than the age estimated by Lachaume et al. (1999).

**$\beta$  Com:** This is a G0 V star with a rotation period of about 12 days (Gray & Baliunas 1997). Temperature and metal abundance (slightly super-solar) were determined by Barklem et al. (2002) and Gray et al. (2001) from spectroscopic analyses. Using the observed data, the evolutionary models of Girardi et al. (2000) yield a mass about 10% larger than the Sun and an age of  $2.3 \pm 1.1$  Gyr, in agreement with the remark of Gray & Baliunas (1997) about  $\beta$  Com being younger than the Sun. To refine the age estimate, we have made use of the rotation period–age relationship for solar-type stars of Guinan et al. (1998) and derived a value of  $\sim 1.6$  Gyr.

**$\beta$  Hyi:** As pointed out by Dravins et al. (1998),  $\beta$  Hyi, of spectral type G2 IV, is our nearest subgiant star. A detailed study of  $\beta$  Hyi was published by Fernandes & Monteiro (2003), who also review determinations of stellar parameters, including the mass and age of  $\sim 6.7$  Gyr. We adopt the values in that recent work. The rotation period of  $\beta$  Hyi was determined from the analysis of 18 IUE High Dispersion LWP spectra obtained during 1994/95 by Guinan under program SPREG. Measures of the chromospheric Mg II h&k emission line fluxes relative to the adjacent continuum were made. The analysis reveals an apparent modulation in the relative Mg II h&k emission strength of  $P_{\text{rot}} = 29 \pm 3$  days arising from chromospheric faculae and plages on the star (Guinan et al. 2005, in prep.).

There is an additional important issue yet to be addressed and this is the interstellar medium (ISM) column density along the targets' lines of sight. Although the stars in the sample are nearby and have negligibly small values of  $E(B-V)$  from ISM dust, some of the studied stellar emission features suffer strong ISM absorption and appropriate corrections need to be applied. The H I column densities in the lines of sight of our targets were estimated from the various lines of sight sampled by the H I Lyman  $\alpha$  observations of Wood et al. (2004). For  $\kappa^1$  Cet and  $\chi^1$  Ori direct measurements are available, whereas for the other four stars we employed the measured H I column densities for neighboring stars (selected on the basis of a similar distance and position). We used HD 116956 for EK Dra, DK UMa for

$\pi^1$  UMa, HZ 43 for  $\beta$  Com, and  $\zeta$  Dor,  $\epsilon$  Ind, and HD 203244 for  $\beta$  Hyi. The total adopted H I column densities in the target lines of sight are given in Table 1. These can be eventually scaled to compute the column densities of other elements from mean local ISM abundances.

### 3. OBSERVATIONAL DATA

Observations of the target stars in Table 1 were carried out with a variety of space-based instruments to maximize spectral coverage. Data from the following space missions have been used in the present study: *Advanced Satellite for Cosmology and Astrophysics* (ASCA), *Röntgen Satellite* (ROSAT), *Extreme Ultraviolet Explorer* (EUVE), *Far Ultraviolet Spectroscopic Explorer* (FUSE), *Hubble Space Telescope* (HST), and *International Ultraviolet Explorer* (IUE). As can be seen in the summary presented in Table 2, the observations discussed in this paper cover approximately the interval between 1 Å and 1700 Å, except for a gap between 360 Å and 920 Å, which is a region of very strong ISM absorption (H I Lyman continuum), thus far largely unexplored for stars other than the Sun. The number of datasets used for this study is quite extensive and thus all observation identification files for each target and mission are listed in Table 3. All the observations described here, both from our guest observer programs and public datasets, were downloaded from the HEASARC<sup>5</sup> and MAST<sup>6</sup> archives.

#### 3.1. X-rays: ASCA & ROSAT

A key aspect of the study is the transformation of the instrumental fluxes into absolute fluxes, which is especially critical for the X-ray data. The observations obtained with ASCA and ROSAT are not naturally in absolute flux units and have to be compared with a physical plasma emission model to perform the calibration. The ASCA observations were obtained with the SIS0 and SIS1 detectors (Tanaka et al. 1994) and pointed observations with the PSPC instrument (Briel & Pfeffermann 1986) were used with ROSAT. We reduced the X-ray data in the classical manner with the XSELECT V2.2 and XSPEC 11.3.0 packages within FTOOLS. Then, as is commonly done for coronal emissions (such as those from our solar analogs), we considered a multi- $T_e$  plasma and ran a  $\chi^2$  optimization fit with the MEKAL model (Mewe et al. 1995). In this procedure we followed the exact same prescriptions as in Güdel et al. (1997a), and adopted plasma models with 2 and 3 components (obtaining results entirely consistent with this earlier study). Then, absolute fluxes were calculated from the best-fitting model with the aid of the XSPEC package. A correction for the H I column density – using the values given in Table 1 – was also included. A plot comparing the X-ray fluxes (ASCA and ROSAT) for the target stars is shown in Figure 1, where large differences (of up to a thousand-fold) become evident. Note that  $\chi^1$  Ori only had ROSAT observations taken with the Boron filter (see footnote to Table 3). We decided not to use these here because of some calibration issues. Güdel et al. (1997a), however, did analyze these data and obtained nearly the same parameters as for  $\pi^1$  UMa (see their tables 3 and 5), as expected from their similar ages.

#### 3.2. EUV: EUVE

EUV observations of some of the targets were carried out as part of the EUVE mission (Malina & Bowyer 1991). In this

<sup>5</sup><http://heasarc.gsfc.nasa.gov/>

<sup>6</sup><http://archive.stsci.edu/>

case, the resulting data can be directly flux calibrated during reduction and thus no emission model has to be assumed beforehand. Data reduction of the EUVE spectra was carried out following the same procedure as in Güdel et al. (1997b). The only detail worth mentioning here is the correction of the H I column density, for which we assumed the values listed in Table 1. An illustration of the EUV fluxes for the observed targets is presented in Figure 2. The spectra of  $\pi^1$  UMa and  $\chi^1$  Ori, which correspond to the same stellar age, were averaged together. Note that most of the output stellar flux is associated with emission lines of highly-ionized element transitions.

### 3.3. FUV: FUSE

To obtain irradiances in the FUV we carried out observations with FUSE using its large aperture (Moos et al. 2000). For a detailed description of the datasets used and the reduction procedure the reader is referred to Guinan et al. (2003), and thus we shall skip the discussion here. The reductions in Guinan et al. also included the correction of ISM absorption in the emission features whenever necessary. To illustrate the irradiance differences among the observed targets, we show a detail of FUSE spectra in Figure 3. The complete FUSE spectra are not shown for the sake of clarity (see Guinan et al. 2003 for the identification of the strongest features) and the region illustrated is a wavelength window around two strong O VI emission lines. Again, a steep flux decrease with increasing age is evident.

### 3.4. UV: IUE & HST

UV spectroscopic observations of two of the stars in Table 1 ( $\chi^1$  Ori and  $\kappa^1$  Cet) were obtained with HST within program #8280. Thanks to the small aperture and the large spectral resolution used (STIS/E140M echelle grating and  $0.^{\prime\prime}2 \times 0.^{\prime\prime}2$  aperture), these observations are ideally suited to study the strong H I Ly $\alpha$  emission line, besides other emission lines in the UV. The estimation of the integrated flux of the H I Ly $\alpha$  line requires careful correction for interstellar H I and D I absorption, which is significant even for the low column densities of our targets. Full details on this procedure and the datasets used can be found in Wood et al. (2004). A comparison of the H I Ly $\alpha$  emission features (with both the observed and rectified line profiles) for the two targets observed is shown in Figure 4.

The UV irradiances of the target stars up to 1700 Å were completed with IUE short wavelength camera (SWP) low-dispersion observations (e.g., Kondo et al. 1989). Flux-calibrated data files are available from the MAST archive following the NEWSIPS calibration pipeline (Nichols & Linsky 1996). However, further correction to the fluxes was applied in accordance with the investigation of Massa & Fitzpatrick (2000). The bulk of the flux in the UV region shortwards of 1700 Å is in the form of emission lines, with negligibly small photospheric continuum contribution. The comparison in Figure 5 depicts IUE spectra of the observed stars, where the decrease of emission line fluxes with age is apparent. The strongest features in the IUE range are labeled in Figure 5 and correspond to: O I  $\lambda 1304$  (triplet), C II  $\lambda 1335$  (triplet<sup>7</sup>), Si IV  $\lambda 1400$  (doublet), C IV  $\lambda 1550$  (doublet), He II  $\lambda 1640$  (multiplet), and C I  $\lambda 1657$  (multiplet). As mentioned above an important issue for some of the emission lines is the correction of ISM absorption. Given the low electron density in the ISM

(e.g., Spitzer & Fitzpatrick 1993; Wood & Linsky 1997), only transitions involving ground levels are expected to experience noticeable ISM absorption. All of the emission features listed above have at least one ground level transition component except for He II  $\lambda 1640$ . In the case of the lines of Si IV, C IV, and C I, the very low abundance of these species in the ISM (largely dominated by C II and Si II; see Wood et al. 2002b) implies negligible absorption in the lines of sight of our targets, rendering any correction unnecessary. In the case of the O I  $\lambda 1304$  and C II  $\lambda 1335$  triplets, one of the components has a ground state transition that is prone to ISM absorption, which we corrected as explained below.

To complement the IUE UV data we made use of the HST echelle spectra described above for  $\chi^1$  Ori and  $\kappa^1$  Cet, which cover a wavelength interval from 1150 to 1700 Å. These higher resolution data served the double purpose of cross-checking the integrated fluxes and carrying out a direct correction for ISM absorption. Inspection of the line profiles indicate that ISM absorption is present in the O I  $\lambda 1302.17$  and C II  $\lambda 1334.53$  components. These account for about 30% and 40% of the total flux of the O I and C II triplets, respectively. We carried out a reconstruction of the line profiles assuming a gaussian functional form with a superimposed absorption (a total of six free parameters). For  $\kappa^1$  Cet, the difference in radial velocity between the star and the ISM components is of only  $\sim 5$  km s $^{-1}$ , thus implying significant absorption. In this case, the corrections to the total O I  $\lambda 1304$  and C II  $\lambda 1335$  fluxes were of 14% and 20% respectively. The resulting profile reconstruction parameters were found to agree very well with the ISM properties in the  $\kappa^1$  Cet line of sight (Wood et al. 2004). For  $\chi^1$  Ori, the radial velocity difference between the star and the absorbing ISM is  $\sim 36$  km s $^{-1}$ , which makes the flux correction negligible (<2%). Approximate corrections for the rest of the stars were computed from the results on  $\chi^1$  Ori and  $\kappa^1$  Cet and the properties of the ISM absorbing components in Wood et al. (2004) – using the line of sight proxies discussed in §2. The resulting corrections to the total O I  $\lambda 1304$  and C II  $\lambda 1335$  fluxes were in the range 2–17%.

### 3.5. Solar irradiance

Finally, we shall describe the mean solar irradiance spectrum used in our comparisons. As a consequence of an increasing number of sounding rocket experiments and space missions, the knowledge of the Sun's high-energy emissions has improved considerably in recent times. In our investigation we have made use of the detailed irradiances constructed by Woods et al. (1998 and references therein) from measurements made by sounding rockets and the UARS SOLSTICE mission. The data products available<sup>8</sup> include low-resolution (10 Å) spectra and line-integrated fluxes for 1992, 1993, and 1994, and a high-resolution (1 Å) spectrum for 1994. All these years correspond to Solar Cycle 22, with 1992 and 1993 representing moderate solar activity levels, and 1994 representing the quiet Sun. We used data from 1993, which corresponds to mid cycle, as representative of the Sun at the “average” activity level. The rocket and UARS SOLSTICE observations cover a wavelength interval from 20 to 2000 Å. Because of the relatively low resolution of the observations ( $\sim 2$  Å), we used the higher resolution solar data from the SMM/UVSP atlas<sup>9</sup> and the high-resolution spec-

<sup>7</sup>One of the components is very weak and separated only 0.04 Å from a strong component.

<sup>8</sup>See [http://lasp.colorado.edu/rocket/rocket\\_results.html](http://lasp.colorado.edu/rocket/rocket_results.html)

<sup>9</sup>[ftp://umbra.nascom.nasa.gov/pub/uv\\_atlases/](ftp://umbra.nascom.nasa.gov/pub/uv_atlases/)

trum of  $\alpha$  Cen A of Pagano et al. (2004) to check for possible contamination by blends in the interval  $\lambda > 1300$  Å. Complementary soft X-ray irradiance measurements from the SNOE experiment (Bailey et al. 2000) were also used in the interval 20–200 Å. To complete the necessary short wavelength data (hard X rays), we made use of the inferred solar flux in the ASCA wavelength interval (1–20 Å) by Güdel et al. (1997a). The resulting energy distribution is in general good agreement with the measurements made by the GOES 10 & 12 satellites in the narrower 1–8 Å range.

#### 4. MEASUREMENT AND ESTIMATION OF IRRADIANCES

One of the ultimate goals of the “Sun in Time” project is to produce a set of data products describing the high-energy irradiance evolution of the Sun and solar-type stars across the main sequence. These fluxes can then be used as an input to model Solar System planet and exoplanet atmospheres and study their variations over time. To present the observational data described in §3 we distinguish two separate components: Integrated fluxes in wide wavelength intervals (roughly defined by the intervals covered by different missions) and emission fluxes of the strongest features in the high-energy spectrum. Data for five representative age stages are given: 100 Myr (EK Dra), 300 Myr ( $\pi^1$  UMa and  $\chi^1$  Ori), 650 Myr ( $\kappa^1$  Cet), 1.6 Gyr ( $\beta$  Com), 4.56 Gyr (Sun), and 6.7 Gyr ( $\beta$  Hyi). In the case of 300 Myr, with two stellar proxies, we scaled the fluxes and computed averages whenever data for the two stars were available.

##### 4.1. Integrated irradiances

The intervals considered are: 1–20 Å (ASCA), 20–100 Å (ROSAT), 100–360 Å (EUVE), and 920–1180 Å (FUSE). Above 1180 Å we provide only the fluxes of the strongest features because of the difficulty in achieving a reliable total integration (caused by the increasing photospheric contribution). We will address this issue in a forthcoming publication. The total fluxes of the observed spectra were corrected to a distance of 1 AU and scaled (using a simple radius-squared relationship) to the expected radius of the Sun at the star’s age (in Table 1). The resulting stellar fluxes are presented in Table 4 (values not in parentheses in the first five rows).

The measured fluxes show excellent correlations with the stellar ages (or, equivalently, with the rotation periods). The analysis reveals that the stellar fluxes can be very well approximated by power-law relationships, as illustrated in Fig. 6a-d. The parameters of the power-law fits are given in Table 5. Interestingly, the slopes of the best-fitting relationships are seen to decrease monotonically from the X-rays to the UV (i.e., decreasing energy or increasing wavelength). Thus, emissions associated with hotter plasmas are found to diminish more rapidly and the overall plasma cools down as the stars spin down with age. This behavior was already reported by earlier studies such as those by Ayres et al. (1981) and Ayres (1999). Ayres (1997) gives also relationships for the relative flux variations at different wavelengths.

As noted previously, the available observations are not complete because of two chief reasons. First, there is a gap between 360 and 920 Å for stars other than the Sun, and second, measurements could not be obtained for all targets in all wavelength intervals. The following targets have observations missing in some wavelength intervals: EK Dra (FUSE),  $\beta$  Com (EUVE, FUSE),  $\beta$  Hyi (EUVE, FUSE). Note that, in the case of FUSE observations, the lack of total flux values is caused

by the impossibility of calculating the flux contribution from the H Lyman lines because of strong geocoronal contamination and saturated interstellar absorption (see Guinan et al. 2003 for further explanation). In the case of EUVE, two of the targets were not observed because their predicted fluxes were below the detection limit of the instrument.

Having a (rough) estimate of the flux emitted by the stars in the intervals not covered by observations is rather critical, especially if the irradiances calculated in this work are to be used as input data in planetary atmosphere modeling. The estimation of fluxes for stars with no FUSE or EUVE observations is straightforward since the derived power laws can be employed to make predictions. Using this procedure we calculated the predicted fluxes in Table 4 (values in single parentheses in the first four rows) and a power-law fit to the integrated fluxes in the wavelength interval covered by the observations (Fig. 6e). With regards to the 360–920 Å interval, no expectations exist of having any observational data, even in the medium-term future. To circumvent the problem, there are at least three possible alternatives: 1) Using empirical irradiances for the Sun with some *ad hoc* scalings to account for the various activity levels of our targets; 2) modelling from EUVE and UV by extrapolation under the assumption that the lines and the continuum are from the same plasma components; or 3) inferring the total integrated flux in the interval by comparison with the flux evolution in other wavelength ranges. We took the third approach chiefly because the accuracy we require is not very high (some 10–20% is sufficient as discussed below). In this way we avoid the use of solar data not suitable to the very high activity level of some of our targets. Also, the second method involves extrapolation from an incomplete range of plasma temperatures since the observations only cover coronal temperatures ( $\sim$  MK) and the temperatures of a few FUV lines ( $\sim 10^5$  K). Given the power-law slopes in Table 5 for different wavelength regions, a value of  $-1.0$  seems to be a good compromise in the 360–920 Å interval. Thus, we calculated the flux predictions in Table 4 (values in double parentheses) from the observed solar flux in this interval and the inferred power-law relationship. This crude interpolation could be flawed if strong emission lines were present in the wavelength interval. This does not seem to be the case when inspecting spectra from the Sun – such as the SOLSTICE data (see §3.5) or the SOHO/SUMER spectral atlas (Curdt et al. 2001) – and from Procyon (Drake et al. 1995), but caution should be exercised when using the tabulated fluxes.

From the estimations described above, we were able to compute total irradiances in the interval 1–1180 Å as given in the last row of Table 4. Also, in Fig. 6f we plot the total integrated fluxes and a power law fit that is found to yield an excellent fit to the data. An illustration of the spectral energy distribution of the targets is provided in Fig. 7, where the solid lines represent the observed data and the dotted lines have been calculated via power-law interpolation. In the complete wavelength interval, which is frequently used in aeronomy calculations, the flux ( $F$ ) as a function of stellar age ( $\tau$ ) is accurately reproduced by the expression (the upper wavelength limit can be extended from 1180 to 1200 Å because there are no additional relevant emission lines):

$$F = 29.7 \cdot [\tau(\text{Gyr})]^{-1.23} \text{ erg s}^{-1} \text{ cm}^{-2}; \quad 1 \text{ Å} < \lambda < 1200 \text{ Å} \quad (1)$$

Also illustrative is the plot in Fig. 8, which represents the stellar fluxes normalized to the current solar values as a function of

age. The steeper decrease of the higher energy emissions is evident in this plot. Also note that the emissions of the youngest stars in all wavelength intervals are orders of magnitude larger than the current solar flux.

#### 4.2. Line fluxes

Line integrated fluxes were measured for the strongest features of the high-energy spectrum whenever possible (i.e., with sufficiently high instrumental resolution). As explained above, the observed fluxes were corrected for interstellar absorption (if necessary), scaled to a distance of 1 AU and to the expected radius of the Sun at the star's age. The resulting line fluxes are presented in Table 6. Note that, as mentioned in §3.5, the fluxes of the Sun for lines with  $\lambda > 1300$  Å were checked for blends with high-resolution spectra. We found any contamination to be below a negligible 10% and no further action was taken.

Similarly to the total integrated fluxes, the line fluxes in Table 6 are also observed to follow well-defined power law relationships as a function of stellar age, with the slopes given in Table 7. Also listed in this table are the characteristic ion formation temperatures, which can be regarded as the typical temperatures of the plasma where the line emissions are originating (Arnaud & Rothenflug 1985). Similarly to the integrated emissions, the flux decrease with age becomes more pronounced with higher formation temperatures (or, generally, shorter wavelengths).

Worth noting here is the powerful H I Lyman  $\alpha$  emission feature. As can be seen by comparing Tables 4 and 6, Ly $\alpha$  is a very significant contributor to the short-wave emission in the Sun and solar-type stars. This sole emission line produces a large fraction of the total flux between 1 and 1700 Å: from about 20% at 100 Myr up to over 50% for the current Sun. The observational data on Ly $\alpha$  irradiances of solar-type stars are still scarce, with only two targets measured thus far. The preliminary results presented here yield the following expression:

$$F = 19.2 \cdot [\tau(\text{Gyr})]^{-0.72} \text{ erg s}^{-1} \text{ cm}^{-2}; \quad \text{H I Lyman } \alpha \quad (2)$$

Note that the formation temperature of this line is about 10 kK and so the power-law slope should be less steep but similar to that in the 920–1180 Å range, exactly as found (cf. Table 5). For comparison, the results of Wood et al. (2004) (i.e.,  $F(\text{Ly}\alpha) \propto P_{\text{rot}}^{-1.09 \pm 0.08}$ ), when combined with the age–rotation period relationship of Ayres (1997) (i.e.,  $P_{\text{rot}} \propto \tau^{-0.6 \pm 0.1}$ ), yield  $F(\text{Ly}\alpha) \propto \tau^{-0.65 \pm 0.12}$  for F and G dwarfs. It is worth noting that this slope is in remarkably good agreement with the value we find.

Some studies have also revealed correlations between certain line fluxes and the overall high-energy flux. This is the case of Bruner & McWhirter (1988), who reported a tight correlation between the C IV  $\lambda 1550$  flux and the total radiated power by solar active regions. We have carried out a similar comparison between the C IV  $\lambda 1550$  flux and the total integrated flux in the 1–1200 Å interval (cf. table 7 and figure 8a of Bruner & McWhirter 1988). The power-law fit has a remarkable correlation coefficient of 0.998 and yields a slope of  $1.12 \pm 0.04$  (i.e.,  $F_{\text{tot}} \propto F_{\text{CIV}}^{1.12}$ ), in good agreement with the value 1.08 obtained by Bruner & McWhirter (the somewhat steeper slope in our case is likely due to the non-inclusion of the UV flux, which would flatten the relationship). This is a strong argument in favor that the emissions of our targets arise from active regions that are similar in nature to those of the Sun.

## 5. DISCUSSION

The comprehensive investigation presented here unequivocally demonstrates that the Sun has experienced a strong decrease of its high-energy emissions over the course of its main sequence evolution. Quantitatively, the results indicate that the solar high-energy flux in the interval 1–1200 Å was about 2.5 times the present value 2.5 Gyr ago and about 6 times the present value about 3.5 Gyr ago. Also, the 100 Myr ZAMS Sun should have had high-energy emissions some 100 times larger than presently in this wavelength interval. The great diminishing of the solar high-energy flux with time is vividly illustrated by the following fact: EK Dra's flux in the sole C III  $\lambda 977$  emission line is larger than the entire integrated current solar irradiance below 1200 Å.

The results also show that an important contributor to the high-energy emissions of solar-type stars is the strong H I Ly $\alpha$  feature. This statement remains true throughout the lifetime of the stars, although the relative fraction of Ly $\alpha$  photons with respect to the high-energy emissions increases with the age of the star. This investigation shows that the Ly $\alpha$  flux 2.5 Gyr and 3.5 Gyr ago was larger than today by factors 1.8 and 2.9, respectively. Again, the 100 Myr old Sun was much more active, with an expected Ly $\alpha$  flux some 15 times larger than presently.

Note that the stellar sample we used covers the solar irradiance evolution from an age of about 100 Myr after its arrival on the main sequence. There are numerous indications that the Sun was even more active during the T Tauri and the early post-ZAMS stages (e.g., Simon et al. 1985, and references therein). Studies indicate that the X-ray luminosity of solar-type stars reaches a saturation level ( $\log L_X/L_{\text{bol}} \approx -3$ ) at a rotation period of about 1.5 d (Pizzolato et al. 2003). The X-ray emission of the youngest, most active solar type stars can be up to 2–3 times higher than the flux of our youngest solar proxy, EK Dra. This is observed in stars of clusters such as  $\alpha$  Per or IC 2391, with ages around 50 Myr. Analogous, saturation effects are expected for the emissions in the EUV and UV ranges. The evolutionary stages younger than 100 Myr have strong significance on stellar evolution, dynamo theory, but also on the ionization of the accretion disk, hence on the planetary formation, and on the astrochemistry. However, these early stages do not bear special relevance to studies related to planetary atmospheres and environments since planets were still forming in the protoplanetary nebula (Chambers & Wetherill 1998; Lissauer 1993). Even somewhat later in the evolution (up to  $\sim 500$  Myr), the influence of the strong solar irradiance may have been overwhelmed by the heavy bombardment period in the inner Solar System (Sleep et al. 1989) as well as planetary meltdowns and volcanism.

#### 5.1. Previous studies

Similar previous works on the same subject were published by Zahnle & Walker (1982) and Ayres (1997). The study of Zahnle & Walker (1982) focused on the evolution of solar ultraviolet emissions and was triggered by the early discoveries of high XUV luminosities of young late-type stars made by the IUE and Einstein satellites. The authors used T Tauri (pre-main sequence) stars and the current solar flux values to interpolate a flux evolution law for different wavelength intervals assuming a  $t^{-1/2}$  scaling law for the rotational velocity. The results are in reasonable agreement with ours, in spite of the fact that Zahnle & Walker did not use a true solar analog sample and employed just two fiducial points for the interpolation. Ayres (1997) carried out a very detailed study of the solar high-energy flux, including a photoionization model for four species (H, O,

$\text{O}_2, \text{N}_2$ ) mostly focused on its application to the primitive Martian atmosphere. The author used a combination of empirical data (EUVE) with global scalings of the solar spectrum using power-laws with slopes depending on the typical temperature formations of the studied ion species. In spite of the different approach, the results by Ayres are in general good agreement with ours. Perhaps the power-law slopes reported by Ayres are slightly smaller, yet still compatible with those presented here.

### 5.2. Uncertainties, cycles, and variability

We have presented in §4 the results of our XUV observations, but no error estimates have been discussed yet for the flux values. There are four chief sources of uncertainty in the stellar fluxes provided (if we neglect the errors associated with the radius and ISM absorption corrections): the measurement errors, the intrinsic variability of the emission, and the scatter associated to the selection of the stellar proxies (i.e., we are assigning a single flux to a mass or spectral type interval). In turn, the error of the measurement has a contribution from the flux integration itself (photon noise) and from the calibration of the detector. The numerical error of the flux integration follows from the propagated error of the the flux uncertainty in each wavelength bin.

We have carried out the necessary calculations and find that the observations were made with sufficiently long integration times so that the photon noise contributes to an uncertainty of less than 5% on the measured fluxes. The exceptions to this are the integrated FUV fluxes, which have strong geocoronal contamination and had to be inferred from alternative methods (see Guinan et al. 2003) resulting in uncertainties of 20–40%, and the ROSAT X-ray flux of  $\beta$  Hyi, with an uncertainty of about 10% due to the low count rate. The estimation of the calibration errors is quite often not straightforward. From the comparison between different X-ray missions and the absolute effective area calculations one deduces an absolute calibration uncertainty of the order of 10–20% for both ASCA SIS and ROSAT PSPC detectors (see documentation in <http://heasarc.gsfc.nasa.gov/>). In the case of EUVE, Bowyer et al. (1996) report that the effective area calibration of each band is believed to be accurate to within 20%. For the FUSE LWRS LiF and SiC detectors, the absolute calibration of the fluxes has an uncertainty below 10% according to the documentation in the FUSE website<sup>10</sup>. Detailed documentation is available on the absolute photometric accuracy of HST STIS/MAMA echelle observations (as those used here) and the expected value is around 8% (see Space Telescope Imaging Spectrograph Instrument Handbook at <http://www.stsci.edu/hst/stis/documents> and also Bohlin 1998). Finally, comparisons indicate that, after correction of systematic effects, the absolute calibration of IUE is accurate to within 3% (Massa & Fitzpatrick 2000).

Summarizing, we estimate that the measurement errors (including both photon noise and absolute calibration uncertainty) of the fluxes in Tables 4 and 6 decrease from about 10–15% in the X-ray domain to about 5–8% in the UV.

As mentioned above, there are additional sources of uncertainty caused by the intrinsic variability of the emission and by the differences between stars in the studied spectral range. Recall that the ultimate goal of this study is to obtain XUV fluxes for the Sun and solar-type stars over their (magnetic) evolutionary histories using stellar proxies. We are interested in obtaining the “average” XUV emissions that are characteristic of

stars in a specific mass or spectral type window (G0–5). With the available observations, there is very little we can say about the scatter caused by using stars that are slightly more massive than the Sun (see Table 1) as proxies. However, there are two competing effects that may cancel each other to a certain extent. On the one hand, more massive stars have larger surface areas and thus larger integrated emissions but, on the other hand, they also have shallower convective zones and a somewhat weaker dynamo. We may speculate that, at first order, the emissions of stars within a small interval in masses are very similar.

But certainly, the main contributor to the uncertainty of the fluxes in Tables 4 and 6 is caused by the intrinsic variability. It is well known that stellar magnetic activity is characterized by short- and mid-term variations over timescales of hours, days, months, and years. It is beyond the scope of this paper to analyze in detail the flux variations of all our solar proxies over these timescales because that would imply a very large observational effort. In most cases, the available observations represent just a “snapshot” of the flux emissions without any reference to the “average” value and its scatter. We may, however, make an educated guess at the amplitude of the variations over timescales of years. In the Sun, besides flares, which are discussed below, the relevant source of mid-term variability is the 11-yr activity cycle (see Lean 1997 for a complete review). In spite of the lack of accurate solar XUV variability measurements yet, the available data indicate solar maximum vs. minimum (i.e., peak to peak) flux ratios of 10–20 for X-rays (10–100 Å) decreasing to ratios of about 2 at 600 Å and 1.2 at 1500 Å (Hinteregger 1981; Rottman 1988; Lean 1997). In the case of the H I Lyman  $\alpha$  emission line, Woods et al. (2000) carry out a detailed study over different timescales and report a solar-cycle peak-to-peak flux ratio of 1.5. The variability factor shows a positive correlation with the temperature of the associated emitting plasma. Thus, for specific lines, the flux variations are a function of their formation temperatures (see Ayres 1997).

Solar-like stars have also been observed to exhibit activity cycles similar in length to that of the Sun (e.g., Baliunas & Vaughan 1985). For example, there is some yet inconclusive evidence for a 10–12 yr X-ray activity cycle in the case of EK Dra (Güdel et al. 2003) and a cycle of similar length in  $\beta$  Hyi (Guinan, unpub). Interestingly, however, the flux maximum vs. minimum ratio for EK Dra in the ROSAT band (i.e.,  $\approx$ 6–120 Å) is about 2.5, or some 4 times smaller than the Sun’s value (e.g., Hempelmann et al. 1996; Micela & Marino 2003). This may just be a consequence of the smaller contrast between maximum and minimum when the stars have high activity levels (i.e., surface active regions) at all times. Indication for possible long-term modulation depths can be obtained by observing cluster stars repeatedly, separated by several years. Such studies have, for example, been performed for the Pleiades cluster that contains many stars somewhat similar to EK Dra, or for the Hyades, similar in age to  $\kappa^1$  Cet. These observing programs typically reported variations of no more than a factor of two for most stars, see, for example, Gagné et al. (1995), Micela et al. (1996), and Marino et al. (2003) for the Pleiades and Stern et al. (1994) and Stern et al. (1995) for the Hyades.

The flux intrinsic variability with the activity cycle of our solar proxies will be the subject of a forthcoming study when the time baseline of the data permits a detailed investigation. At this point, taking into account all the available information, we

<sup>10</sup>[http://fuse.pha.jhu.edu/analysis/calfuse\\_wp0.html](http://fuse.pha.jhu.edu/analysis/calfuse_wp0.html)

estimate total uncertainties for the power-law slopes in Table 5 no larger than 0.1.

A further source of short-term variability are stellar flares. These are important to certain applications of our irradiance data because the amount of energy released in a single event can be significant. Observations of some of the solar proxies in our stellar sample indicate that flare events in young solar proxies such as EK Dra are frequent ( $\sim 3\text{--}4$  major flares per day) and up to 100 times more powerful than observed for the present Sun (Audard et al. 1999). X-ray flaring has also been observed on  $\pi^1$  UMa and a large X-ray flare (ten-fold X-ray enhancement) was recorded by the EXOSAT satellite during January 1984 (Landini et al. 1986). Another of our targets,  $\kappa^1$  Cet, experienced a flare that was recorded spectroscopically in the visible by Robinson & Bopp (1987). For an up-to-date study of X-ray flaring (which includes new observations of some of our targets) the reader is referred to the recent paper by Telleschi et al. (2005). Also, we plan in the near future to use recently acquired time-tagged spectra with FUSE to address the evolution of the flare rates and energetics of solar-type stars over their lifetimes. We stress that the fluxes given in this paper are clear of major flare events and should constitute a faithful representation of the quiescent emission of the targets.

### 5.3. Particle fluxes

With enhanced high-energy emissions and frequent flares, young solar-type stars are also expected to have more powerful particle winds. Evidence from lunar and meteoritic fossil record agrees with this extrapolation and suggests that the Sun had a stronger wind in the past (e.g., Newkirk 1980). Similar conclusions were drawn by Lammer et al. (2000) from the study of the  $^{15}\text{N}/^{14}\text{N}$  isotope ratio in the atmosphere of Titan. The indirect evidence of an enhanced particle flux during the first 500 Myr of its life would be more compelling if a direct detection of the wind of a solar-type star was attained. Attempts made by Gaidos et al. (2000) to detect the winds of  $\pi^1$  UMa,  $\kappa^1$  Cet, and  $\beta$  Com from their radio emissions yielded negative results. Also unsuccessful was the search for blue-shifted absorption in coronal lines carried out by Ayres et al. (2001).

Although winds of solar-like stars have not yet been detected directly, Wood et al. (2001, 2002a) devised a method to infer their characteristics from observations of the interaction between the fully ionized coronal winds and the partially ionized local ISM. Modeling of the associated absorption features, which are formed in the “astrospheres,” has provided the first empirical estimates of coronal mass-loss rates for G–K main-sequence stars. From the small sample where the astrospheres can be observed, the mass loss rates appear to increase with stellar activity. Using simple relationships involving rotational velocities and X-ray fluxes, Wood et al. (2002a) suggest that the mass loss rate of the Sun has decreased following a power law proportional to  $t^{-2}$ , which implies that the wind of the active young Sun may have been around 1000 times more massive than it is today. There are still a number of assumptions that have to be proved before this result can be fully established, especially the correlation between X-ray flux and mass loss rate as these originate from physically distinct regions (closed and open fields, respectively), but Wood et al.’s work is an important step forward.

With many of the solar wind characteristics still being unveiled today, it is not surprising that our knowledge of the particle fluxes of solar-type stars of different ages is at a very basic stage. Evidence from independent sources indicates that

the young Sun (and by extension, young solar-type stars) had a wind significantly more intense than presently. Also, the high frequency of large flares observed with EUVE by Audard et al. (2000) in young Suns such as EK Dra and 47 Cas B could indicate explosive episodic releases of plasma generating non-thermal high-energy particles. These would be like the coronal mass ejections observed on the Sun but hundreds of times stronger and more frequent. Similarly to the Sun today (Lewis & Simnett 2000; Schrijver & Zwann 2000), coronal mass ejections could contribute significantly to the stellar wind. As we discuss below, the solar wind plays an important role in the shaping and evolution of planetary atmospheres and surfaces and thus it is an important component when characterizing the magnetic activity evolution of the Sun over its lifetime.

## 6. APPLICATIONS OF THE SOLAR IRRADIANCE DATA

### 6.1. Thermal escape on exoplanets

The high-energy irradiance evolution data presented in this paper are intended to be an ingredient of studies related to the evolution of Solar System planets and exoplanets. Meier (1991) gives the absorption profile of the Earth’s atmosphere and shows that most of the radiation with  $\lambda \lesssim 1700$  Å is absorbed (and thus deposits its energy) in the thermosphere, at an altitude above 90 km. Similar effects are found in atmospheres with different compositions (e.g., within the Solar System) since the absorption cross-sections of the high-energy photons by all the atomic species present in the upper atmospheres are very large. Thus, XUV ionizing radiation raises the temperature of the planetary thermospheres and affects their vertical temperature profiles and energy transport mechanisms. Obviously, planets around young solar-type stars, with XUV fluxes 10–100 times stronger than today’s Sun, suffer intense heating of their upper atmospheres, that reach temperatures much above the current value of 1000 K for the Earth. When the temperature of the thermosphere is large, a significant fraction of the light constituents of the upper atmosphere attain velocities above the escape value (and drag heavier constituents away).

Thermal escape, although commonly neglected in the present Solar System, may be important in planets around magnetically active stars. Thus, any attempt to calculate the history of a planet’s atmosphere around a solar-type star needs to include the XUV energy evolution, since this regulates the efficiency of evaporation processes. Calculations using early data from the present work were carried out by Lammer et al. (2003b), who showed that “Hot Jupiters” could lose significant fractions of their hydrogen masses under intense XUV radiation. Non-thermal mechanisms caused by ionosphere-stellar wind interactions also contribute to this loss processes (Grießmeier et al. 2004). The tantalizing results indicate that hydrogen-rich giant exoplanets may suffer rapid evaporation under strong XUV radiation conditions. Once the entire hydrogen envelope is lost, only the rocky planetary cores would remain, thus representing a putative new class of planet. The confirmation of the theoretical prediction of thermal escape comes from the observations of Vidal-Madjar et al. (2003), who reported a large exospheric radius for the transiting planet HD 209458 b (due to thermal expansion) and a loss rate compatible with the estimates of Lammer et al. The consequences of this enhanced thermal loss process could explain the apparent paucity of exoplanets so far detected at very close orbital distances ( $< 0.05$  AU). Terrestrial-like planets could also be affected by the enhanced XUV environment and lose a significant fraction of their

lighter atmospheric constituents.

### 6.2. The Martian water inventory

The “Sun in Time” data are also being used to study aspects related to the evolution of Solar System planet atmospheres and surfaces. In particular, the planet Mars has been especially vulnerable in the past to the influence of the Sun’s energy and particle emissions because of its small mass and the lack of a protecting magnetic field. Lammer et al. (2003a) and Terada et al. (2004) have studied the Martian water inventory using reliable solar XUV and wind evolution laws and comprehensive models for the loss processes of hydrogen and oxygen that include dissociative recombination, ion pickup, sputtering, viscous processes in the planet’s ionosphere. The more recent work of Terada et al. uses a global hybrid model to conclude that the loss of  $H_2O$  from Mars over the last 3.5 Gyr is equivalent to a global Martian ocean with a depth of about 10.5 m. This value is smaller than those reported by previous studies but could still be slightly overestimated.

The two studies quoted also find that the sum of thermal and non-thermal atmospheric loss rates of H and all non-thermal escape processes of O to space are not compatible with a ratio of 2:1 (H to O) expected from the atomic composition of water, and is currently close to about 20:1. Escape to space cannot therefore be the only sink for oxygen on Mars. These results suggest that the missing oxygen can be explained by the incorporation into the Martian surface by chemical weathering processes since the onset of intense oxidation about 2 Gyr ago. The oxygen incorporation has also implications for the oxidant extinction depth, which is an important parameter to determine required sampling depths on Mars aimed at finding organic material. The oxidant extinction depth is expected to lie in a range between 2 and 5 m for global mean values.

### 6.3. Erosion of Mercury’s surface

The planet Mercury, because of its closeness to the Sun, has suffered major exposure to the particle and XUV emissions during the early active stages (see Guinan & Ribas 2004). Mercury’s core is large compared to other terrestrial planets, extending out to over 60% of its radius. One of several hypotheses advanced to explain this anomaly is that strong, dense winds and very high XUV fluxes of the young Sun (during the first 0.5–1 Gyr of its life) swept away its early atmosphere and much of its outer mantle. Even today (with a much less active Sun) ground based observations of heavy constituents like  $Na^+$ ,  $K^+$  and  $O^+$  in Mercury’s present transient exosphere implicate a strong exosphere-surface interaction related to the particle and radiation environment of the nearby Sun (e.g., Cameron 1985). Lammer et al. (2002) have carried out initial calculations that indicate that enhanced solar wind and XUV emissions could be sufficient to explain the present relatively thin mantle and relatively large iron core. If this hypothesis is correct, young Mercury may have started out similar in size to the Earth but lost much of its less dense mantle from radiation and particle interactions (ion pick-up) with the young Sun.

### 6.4. The paleo-climate of the Earth

Finally, the young Sun’s emissions may have also had an impact on the early evolution of Earth’s atmosphere. Besides heating the thermosphere and altering the vertical temperature profile, the enhanced high-energy flux can strongly influence the photochemistry and photoionization of the early planetary

atmospheres and also may play a role in the origin and development of life on Earth as well as possibly on Mars. For example, Canuto et al. (1982, 1983) discuss the photochemistry of  $O_2$ ,  $O_3$ ,  $CO_2$ ,  $H_2O$ , etc, in the presumed  $CO_2$ -rich early atmosphere of the Earth. In this context, the  $Ly\alpha$  flux plays an important role as it is strong enough to penetrate the planetary exospheres into their mesospheres, richer in molecules and susceptible to photochemical reactions.

The “Sun in Time” data can also provide insights into the so-called Faint Sun Paradox (see Guinan & Ribas 2002). The paradox arises from the fact that standard stellar evolutionary models show that the Zero-Age Main Sequence Sun had a bolometric luminosity of  $\sim 70\%$  of the present Sun. This should have led to a much cooler Earth in the past while geological and fossil evidence indicate otherwise. A solution to the Faint Sun Paradox proposed by Sagan & Mullen (1972) was an increase of the greenhouse effect for the early Earth. The gases that have been suggested to account for this enhanced greenhouse effect are  $CO_2$ ,  $NH_3$  or  $CH_4$  (see, e.g., Rye et al. 1995; Sagan & Chyba 1997; Pavlov et al. 2000). Although the stronger XUV solar radiation cannot by itself explain the Faint Sun Paradox (because it only accounts for an insignificant percentage of the Sun’s radiative output), the photoionization and photodissociation reactions triggered could play a major role in what greenhouse gases are available. For example, the enhanced photodissociating FUV–UV radiation levels of the young Sun may have influenced the abundances of ammonia and methane in the pre-biotic and Archean planetary atmosphere some 2–4 Gyr ago. Similarly, the photochemistry and abundance of  $O_3$  is of great importance to study life genesis on Earth.

In summary, any model of the paleoatmosphere of the Earth and other Solar System planets needs to account for the stronger XUV and particle radiation from the young Sun. If the XUV fluxes of the young Sun are estimated by a simple scaling of the current values by a factor of 0.7 (in accordance with the lower expected photospheric flux), this will represent a severe underestimation of the radiation levels by orders of magnitude.

## 7. CONCLUSIONS

One of the primary goals of the “Sun in Time” program is to reconstruct the spectral irradiance evolution of the Sun and, by extension, of solar-type stars. To this end, a large number of multiwavelength (X-ray, EUV, FUV, UV, visible) have been collected and analyzed. The observations, secured with the ASCA, ROSAT, EUVE, FUSE, HST, and IUE satellites, cover 1 Å (12 keV) to 1700 Å, except for a gap between 360 Å and 920 Å, which is a region of very strong ISM absorption. Irradiance data are already available for five of the stars in our sample.

A detailed quantitative analysis reveals that the stellar fluxes can be very well approximated by power-law relationships. Interestingly, the slopes of the best-fitting relationships are seen to decrease monotonically from the X-rays to the UV (i.e., decreasing energy or increasing wavelength). Emissions associated with hotter plasmas diminish more rapidly and the overall plasma cools down as the stars spin down with age. The results from the “Sun in Time” program suggest that the coronal X-ray–EUV emissions of the young main-sequence Sun were  $\sim 100$ –1000 times stronger than those of the present Sun. Similarly, the transition region and chromospheric FUV–UV emissions of the young Sun are expected to be 20–60 and 10–20 times stronger, respectively, than presently. In the entire XUV interval from 1 to 1200 Å we find that the solar high-energy flux

was about 2.5 times the present value 2.5 Gyr ago and about 6 times the present value about 3.5 Gyr ago (when life arose on Earth). Also, preliminary estimates using spectra of two solar proxies indicate that Ly $\alpha$  flux of the young Sun was also much stronger, by up to a factor of 15. In addition to intense levels of dynamo generated coronal and chromospheric XUV emissions, the young Sun and young solar analogues are also expected to have stronger and more frequent flares and to have stronger (more massive) stellar winds.

In summary, compelling observational evidence indicates that the Sun underwent a much more active phase in the past. The enhanced activity revealed itself in the form of strong high-energy emissions, frequent flares, and a powerful stellar wind. Such energy and particle environment certainly had an impact on the genesis and evolution of Solar System planets and planetary atmospheres.

Besides completing remaining gaps in the data (e.g., Ly $\alpha$  irradiances; somewhat complicated by the demise of the STIS spectrograph on HST) and better characterizing the flare statistics and wind properties, future work will be directed in two main directions. We plan to extend our study to longer wavelengths between 1700 and 3000 Å. Here the photospheric emissions begin to dominate over those of the chromosphere and a lot more care has to be taken in adequately normalizing the flux. Also, because the emission differences between young and old solar-type stars are expected to be smaller ( $\sim$ 10-30%). The UV portion of the spectrum (UVA, UVB, and UVC) is of great importance as it drives the majority of the photochemical reactions and may influence the generation and destruction of some chemical compounds, e.g., NO<sub>x</sub>, of importance to life.

Because lower-mass stars are especially common and hence may host habitable planets, progress in this direction has started

by expanding the “Sun in Time” program to time sequences of the high-energy emissions, wind, and flare activity of low-mass K and M stars. These stars are far more numerous than the solar-type stars, have long main sequence lifetimes and are, in principle, prime targets for terrestrial planet searches. Because of the low luminosities, their “habitable zones” (see Kasting et al. 1993) can be quite close to the host stars. Low-mass stars have deeper outer convective zones (where the magnetic dynamo operates) than Sun-like stars and thus possess very efficient magnetic dynamos. The expected enhanced XUV radiation environment should play a major role in the development of the atmospheres and ultimately of life on planets located in their habitable zones.

We gratefully acknowledge B. E. Wood for his help with the analysis of the Lyman  $\alpha$  observations. We are also grateful to H. Lammer and F. Selsis for their support to this project and for their interest in using the resulting data. We are very grateful to the referee, Dr. Jeffrey L. Linsky, for his useful suggestions and comments that have led to substantial improvements in the paper. I. R. acknowledges support from the Spanish Ministerio de Ciencia y Tecnología through a Ramón y Cajal fellowship. We acknowledge with gratitude the support for the “Sun in Time” program from NASA grants NAG 5-382 (IUE), NAG 5-1662 (ROSAT), NAG 5-1703 (IUE), NAG 5-2160 (IUE), NAG 5-2494 (ROSAT), NAG 5-2707 (ASCA), NAG 5-3136 (EUVE), NAG 5-8985 (FUSE), NAG 5-10387 (FUSE), and NAG 5-12125 (FUSE). General stellar X-ray astronomy research at PSI has been supported by the Swiss National Science Foundation under projects 2100-049343.96, 20-58827.99, and 20-66875.01. This research has made use of NASA’s Astrophysics Data System.

## REFERENCES

Arnaud, M., & Rothenflug, R. 1985, *A&AS*, 60, 425  
 Audard, M., Güdel, M., Drake, J. J., & Kashyap, V. L. 2000, *ApJ*, 541, 396  
 Audard, M., Güdel, M., & Guinan, E. F. 1999, *ApJ*, 513, L53  
 Ayres, T. R. 1997, *JGR*, 102, 1641  
 Ayres, T. R., Marstad, N. C., & Linsky, J. L. 1981, *ApJ*, 247, 545  
 Ayres, T. R. 1999, *ApJ*, 525, 240  
 Ayres, T. R., Brown, A., Osten, R. A., Huenemoerder, D. P., Drake, J. J., Brickhouse, N. S., & Linsky, J. L. 2001, *ApJ*, 549, 544  
 Bailey, S. M., Woods, T. N., Barth, C. A., Solomon, S. C., Canfield, L. R., & Korde, R. 2000, *JGR*, 105, 27,179  
 Baliunas, S. L., & Vaughan, A. H. 1985, *ARA&A*, 23, 379  
 Barklem, P. S., Stempels, H. C., Allende Prieto, C., Kochukhov, O. P., Piskunov, N., & O’Mara, B. J. 2002, *A&A*, 385, 951  
 Barrado y Navascués, D., Stauffer, J. R., & Randich, S. 1998, *ApJ*, 506, 347  
 Bohlin, R. 1998, *STIS Instrument Science Report* 98-18  
 Bowyer, S., Lampton, M., Lewis, J., Wu, X., Jelinsky, P., & Malina, R. F. 1996, *ApJS*, 102, 129  
 Briel, U. G., & Pfeffermann, E. 1986, in *EUV, X-Ray, and Gamma-Ray Instrumentation for Astronomy VI*, eds. O. H. Siegmund, & J. V. Vallerga, *Proc. SPIE*, Vol. 2518, p. 120  
 Bruner, M. E., & McWhirter, R. W. P. 1988, *ApJ*, 326, 1002  
 Cameron, A. G. W. 1985, *Icarus*, 64, 285  
 Canuto, V. M., Levine, J. S., Augustsson, T. R., & Imhoff, C. L. 1982, *Nature*, 296, 816  
 Canuto, V. M., Levine, J. S., Augustsson, T. R., Imhoff, C. L., & Giampapa, M. S. 1983, *Nature*, 305, 281  
 Chambers, J. E., & Wetherill, G. W. 1998, *Icarus*, 136, 304  
 Cockell, C. S., Catling, D. C., Davis, W. L., Snook, K., Kepner, R. L., Lee, P., & McKay, C. P. 2000, *Icarus*, 146, 343  
 Curdt, W., Brekke, P., Feldman, U., Wilhelm, K., Dwivedi, B. N., Schühle, U., & Lemaire, P. 2001, *A&A*, 375, 591  
 Dorren, J. D., & Guinan, E. F. 1994, in *IAU Coll. 143, The Sun as a Variable Star*, eds. J. M. Pap, C. Fröhlich, H. S. Hudson, & S. K. Solanki (Cambridge: CUP), p. 206  
 Drake, J. J., Laming, J. M., & Widing, K. G. 1995, *ApJ*, 443, 393  
 Dravins, D., Lindegren, L., & Vandenberg, D. A. 1998, *A&A*, 330, 1077  
 Duquennoy, A., & Mayor, M. 1991, *A&A*, 248, 485  
 Durney, B. 1972, in *Solar Wind*, eds. C. P. Sonett, P. J. Coleman, & J. M. Wilcox (Washington: NASA), p. 282  
 Fernandes, J., & Monteiro, M. J. P. F. G. 2003, *A&A*, 399, 243  
 Gagné, M., Caillault, J.-P., & Stauffer, J. R. 1995, *ApJ*, 450, 217  
 Gaidos, E. J., & González, G. 2002, *New A.*, 7, 211  
 Gaidos, E. J., Güdel, M., & Blake, G. A. 2000, *Geophys. Res. Lett.*, 27, 501  
 Girardi, L., Bressan, A., Bertelli, G., & Chiosi, C. 2000, *A&AS*, 141, 371  
 Gratton, R. G., Carretta, E., & Castelli, F. 1996, *A&A*, 314, 191  
 Gray, D. F., & Baliunas, S. L. 1997, *ApJ*, 475, 303  
 Gray, R. O., Graham, P. W., & Hoyt, S. R. 2001, *AJ*, 121, 2159  
 Grießmeier, J.-M., Stadelmann, A., Penz, T., et al. 2004, *A&A*, 425, 753  
 Güdel, M., Audard, M., Smith, K. W., et al. 2003, in *Future of Cool-Star Astrophysics: The Twelfth Cambridge Workshop on Cool Stars, Stellar Systems and the Sun*, eds. A. Brown, G. M. Harper, & T. R. Ayres (Boulder: Univ. of Colorado), p. 303  
 Güdel, M., Guinan, E. F., Mewe, R., Kaastra, J. S., & Skinner, S. L. 1997b, *ApJ*, 479, 416  
 Güdel, M., Guinan, E. F., & Skinner, S. L. 1997a, *ApJ*, 483, 947  
 Guinan, E. F., Güdel, M., & DeWarf, L. E. 1998, in *Solar Analogs: Characteristics and Optimum Candidates*, ed. J. C. Hall (Flagstaff: Lowell Observatory), p. 61  
 Guinan, E. F., & Ribas, I. 2002, in *The Evolving Sun and its Influence on Planetary Environments*, eds. B. Montesinos, A. Giménez, & E. F. Guinan (San Francisco: ASP), *ASP Conference Series*, Vol. 269, p. 85  
 Guinan, E. F., & Ribas, I. 2004, in *IAU Symposium 219, Stars as Suns: Activity, Evolution, and Planets*, eds. A. Benz, & A. K. Dupree (San Francisco: ASP), in press  
 Guinan, E. F., Ribas, I., & Harper, G. M. 2003, *ApJ*, 594, 561  
 Hamilton, R. T., Guinan, E. F., & DeWarf, L. E. 2003, *AAS*, 203.4801  
 Han, I., & Gatewood, G. 2002, *PASP*, 114, 224  
 Hempelmann, A., Schmitt, J. H. M. M., & Stepien, K. 1996, *A&A*, 305, 284  
 Hinteregger, H. E. 1981, *Adv. Space Res.*, 1, 39  
 Kasting, J. F., & Catling, D. 2003, *ARA&A*, 41, 429  
 Kasting, J. F., Whitmire, D. P., & Reynolds, R. T. 1993, *Icarus*, 101, 108  
 King, J. R., Villareal, A. R., Soderblom, D. R., Gulliver, A. F., & Adelman, S. J., 2003, *AJ*, 125, 1980  
 Kondo, Y., Boggess, A., & Maran, S. P. 1989, *ARA&A*, 27, 397

König, B., Fuhrmann, K., Neuhäuser, R., Charbonneau, D., & Jayawardhana, R. 2002, *A&A*, 394, L43

Lachaume, R., Dominik, C., Lanz, T., & Habing, H. J. 1999, *A&A*, 348, 897

Lammer, H., Lichtenegger, H., Kolb, C., Ribas, I., Guinan, E. F., & Bauer, S. J. 2003a, *Icarus*, 165, 9

Lammer, H., Selsis, F., Ribas, I., Guinan, E. F., Bauer, S. J., & Weiss, W. W. 2003b, *ApJ*, 598, L121

Lammer, H., Stumpfner, W., Molina-Cuberos, G. J., Bauer, S. J., & Owen, T. 2000, *P&SS*, 48, 529

Lammer, H., Tehrany, M. G., Hanslmeier, A., Ribas, I., Guinan, E. F., & Kolb, C. 2002, EGS meeting (Nice)

Landini, M., Monsignori Fossi, B. C., Pallavicini, R., & Piro, L. 1986, *A&A*, 157, 217

Lean, J. 1997, *ARA&A*, 35, 33

Lewis, D. J., Simnett, G. M. 2000, *Solar Phys.*, 191, 185

Lissauer, J. J. 1993, *ARA&A*, 31, 129

Malina, R. F., & Bowyer, S. 1991, *Extreme ultraviolet astronomy* (New York: Pergamon Press)

Marino, A., Micela, G., Peres, G., & Sciortino, S. 2003, *A&A*, 406, 629

Massa, D., & Fitzpatrick, E. L. 2000, *ApJS*, 126, 517

Meier, R. R. 1991, *SSRv*, 58, 1

Messina, S., & Guinan, E. F. 2003, *A&A*, 409, 1017

Messina, S., Rodonò, M., & Guinan, E. F. 2001, *A&A*, 366, 215

Metchev, S. A., & Hillenbrand, L. A. 2004, *ApJ*, in press (astro-ph/0408528)

Mewe, R., Kaastra, J. S., & Liedahl, D. A. 1995, *Legacy*, 6, 16

Micela, G., & Marino, A. 2003, *A&A*, 404, 637

Micela, G., Sciortino, S., Kashyap, V., Harnden, F. R. Jr., & Rosner, R. 1996, *ApJS*, 102, 75

Montes, D., López-Santiago, J., Fernández-Figueroa, M. J., & Gálvez, M. C. 2001b, *A&A*, 379, 976

Montes, D., López-Santiago, J., Gálvez, M. C., Fernández-Figueroa, M. J., De Castro, E., & Cornide, M. 2001a, *MNRAS*, 328, 45

Moos, H. W., Cash, W. C., Cowie, L. L., et al. 2000, *ApJ*, 538, L1

Newkirk, G., Jr. 1980, in *The ancient Sun: Fossil record in the Earth, Moon and meteorites*, eds. R. O. Pepin, J. A. Eddy, & R. B. Merrill (New York: Pergamon Press), p. 293

Nichols, J. S., & Linsky, J. L. 1996, *AJ*, 111, 517

Ottmann, R., Pfeiffer, M. J., & Gehren, T. 1998, *A&A*, 338, 661

Pagano, I., Linsky, J. L., Valenti, J., & Duncan, D. K. 2004, *A&A*, 415, 331

Parker, E. N. 1970, *ARA&A*, 8, 1

Pavlov, A. A., Kasting, J. F., Brown, L. L., Rages, K. A., & Freedman, R. 2000, *JGR*, 105, 11981

Pizzolato, N., Maggio, A., Micela, G., Sciortino, S., & Ventura, P. 2003, *A&A*, 397, 147

Porto de Mello, G. F., & da Silva, L. 1997, *ApJ*, 482, L89

Radick, R. R., Lockwood, G. W., Skiff, B. A., & Thompson, D. T. 1995, *ApJ*, 452, 332

Robinson, C. R., & Bopp, B. W. 1987, in *Cool Stars, Stellar Systems and the Sun*, Proceedings of the Fifth Cambridge Workshop, Lecture Notes in Physics, Vol. 291, eds. J. L. Linsky, & R. E. Stencel (Berlin: Springer-Verlag), p. 509

Rottman, G. J. 1988, in *Solar Radiative Output Variation*, ed. P. Foukal (Boulder: NCAR), p. 71

Rye, R., Kuo, P. H., & Holland, H. D. 1995, *Nature*, 378, 603

Schrijver, C. J., & Zwann, C. 2000, *Solar and Stellar Magnetic Activity* (Cambridge: CUP)

Sagan, C., & Chyba, C. 1997, *Science*, 276, 1217

Sagan, C., & Mullen, G. 1972, *Science*, 177, 52

Simon, T., Boesgaard, A. M., & Herbig, G. 1985, *ApJ*, 293, 551

Skumanich, A. 1972, *ApJ*, 171, 565

Sleep, N. H., Zahnle, K. J., Kasting, J. F., & Morowitz, H. J. 1989, *Nature*, 342, 139

Smith, D. S., Scalo, J., & Wheeler, J. C. 2004, *Icarus*, 171, 229

Soderblom, D. R. 1982, *ApJ*, 263, 239

Soderblom, D. R., & Mayor, M. 1993, *AJ*, 105, 226

Spitzer, L., Jr., & Fitzpatrick, E. L. 1993, *ApJ*, 409, 299

Stern, R. A., Schmitt, J. H. M. M., Pye, J. P., Hodgkin, S. T., Stauffer, J. R., & Simon, T. 1994, *ApJ*, 427, 808

Stern, R. A., Schmitt, J. H. M. M., & Kahabka, P. T. 1995, *ApJ*, 448, 683

Strassmeier, K. G., & Rice, J. B. 1998, *A&A*, 330, 685

Tanaka, Y., Inoue, H., & Holt, S. S. 1994, *PASJ*, 46, L37

Taylor, B. J. 2003a, *A&A*, 398, 731

Taylor, B. J. 2003b, *A&A*, 398, 721

Telleschi, A., Güdel, M., Briggs, K. R., Audard, M., Skinner, S. L., Ness, J.-U. 2005, *ApJ*, submitted

Terada, N., Lammer, H., Penz, T., et al. 2004, *Icarus*, in press

Vidal-Madjar, A., Lecavalier des Etangs, A., Désert, J.-M., Ballester, G. E., Ferlet, R., Hébrard, G., & Mayor, M. 2003, *Nature*, 422, 143

Wichmann, R., Schmitt, J. H. M. M., & Hubrig, S. 2003, *A&A*, 399, 983

Wood, B. E., & Linsky, J. L. 1997, *ApJ*, 474, L39

Wood, B. E., Linsky, J. L., Müller, H.-R., Zank, G. P. 2001, *ApJ*, 547, L49

Wood, B. E., Müller, H.-R., Zank, G., & Linsky, J. L. 2002a, *ApJ*, 574, 412

Wood, B. E., Redfield, S., Linsky, J. L., & Sahu, M. S. 2002b, *ApJ*, 581, 1168

Wood, B. E., Redfield, S., Linsky, J. L., Müller, H.-R., & Zank, G. P. 2004, *ApJ*, submitted

Woods, T. N., Rottman, G. J., Bailey, S. M., Solomon, S. C., & Worden, J. R. 1998, *Solar Phys.*, 177, 133

Zahnle, K. J., & Walker, J. C. G. 1982, *Rev. Geophys. Space Phys.*, 20, 280

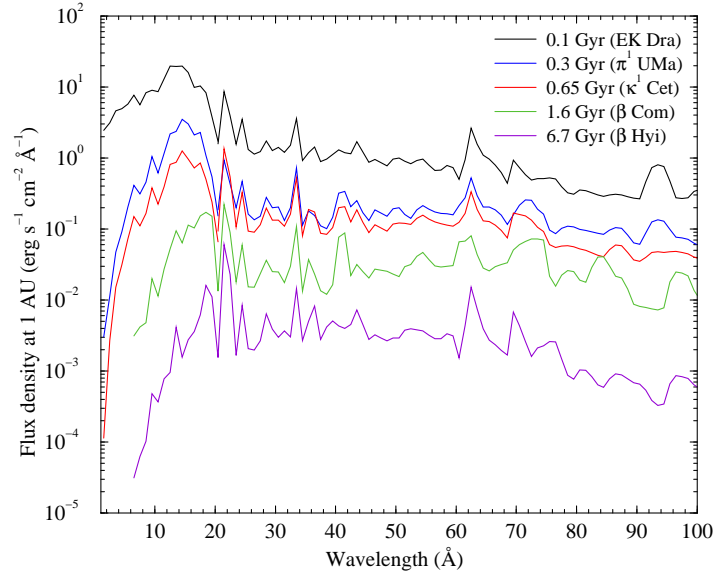


FIG. 1.—X-ray spectral irradiances (flux density at 1 AU vs. wavelength) covering different stages of the evolution of solar-type stars. The plot represents the fluxes in 1 Å bins as predicted by multi-T plasma fits to ASCA and ROSAT observations (see text). Note the very large differences between young and old solar-type stars of up to a factor 1000.

TABLE 1  
RELEVANT DATA FOR THE STUDIED SUN IN TIME TARGETS

Name	HD	Sp. Typ.	d (pc)	$N_{\text{H}}$ ( $\text{cm}^{-2}$ )	$T_{\text{eff}}$ (K)	Mass ( $M_{\odot}$ )	Radius ( $R_{\odot}$ )	Sun R <sup>a</sup> ( $R_{\odot}$ )	$P_{\text{rot}}$ (d)	Age (Gyr)	Age indicator
EK Dra	129333	G1.5 V	34.0	$\sim 1.5 \times 10^{18}$	5870	1.06	0.95	0.900	2.68	0.1	Local Association & Li
$\pi^1$ UMa	72905	G1.5 V	14.3	$\sim 1 \times 10^{18}$	5850	1.03	0.95	0.902	4.90	0.3	UMa group
$\chi^1$ Ori	39587	G1 V	8.7	$9 \times 10^{17}$	5890	1.01	0.96	0.902	5.24	0.3	UMa group
$\kappa^1$ Cet	20630	G5 V	9.2	$8 \times 10^{17}$	5750	1.02	0.93	0.910	9.21	0.65	$P_{\text{rot}}\text{-age}$ & $L_X$
$\beta$ Com	114710	G0 V	9.2	$\sim 1 \times 10^{18}$	6000	1.10	1.08	0.925	12	1.6	$P_{\text{rot}}\text{-age rel.}$
Sun	—	G2 V	1 AU	0	5777	1.00	1.00	1.00	25.4	4.6	Isotopic dating
$\beta$ Hyi	2151	G2 IV	7.5	$\sim 2 \times 10^{18}$	5774	1.10	1.90	1.10	~28	6.7	Isochrones

<sup>a</sup>Radius of the Sun at the same age from the models of Girardi et al. (2000).

TABLE 2  
SUMMARY OF SPACE MISSIONS USED IN THIS INVESTIGATION

Instrument	Wavelength range (Å)	Calibration method
ASCA	1–40	Multi- $T_e$ plasma model
ROSAT	6–124	Multi- $T_e$ plasma model
EUVE	80–760 <sup>†</sup>	Flux calibrated
FUSE	920–1180	Flux calibrated
HST	1150–1730	Flux calibrated
IUE	1150–1950 <sup>††</sup>	Flux calibrated

<sup>†</sup> $\lambda > 360$  Å not useful because of strong interstellar absorption.

<sup>††</sup>Used the SWP camera and for  $\lambda < 1700$  Å only.

TABLE 3  
OBSERVATION DATES AND IDS FOR ALL DATASETS USED IN THIS INVESTIGATION

Target	ASCA		ROSAT <sup>a</sup>		EUVE	
	Date	Obs ID	Date	Obs ID	Date	Obs ID
EK Dra	1994-05-24	22012000	1993-10-19	rp201474n00	1995-12-06	ek_dra_9512061129
$\pi^1$ UMa	1993-11-13	21018000	1993-10-05	rp201472n00	1998-11-30	3_uma_9811301325
					1998-12-05	3_uma_9812050029
$\chi^1$ Ori	–	–	–	–	1993-01-26	chi1_ori_9301261159
$\kappa^1$ Cet	1994-08-16	22013000	1993-07-27	rp201473n00	1994-10-13	kappa_cet_9410131500
					1995-10-06	kappa_cet_9510061036
$\beta$ Com	–	–	1993-06-17	rp201471n00	–	–
$\beta$ Hyi	–	–	1991-04-21	rp200071n00	–	–

Target	FUSE		HST		IUE	
	Date	Obs ID	Date	Obs ID	Date	Obs ID
EK Dra	2002-05-14	C1020501	–	–	1992-05-31	SWP 44817
$\pi^1$ UMa	2001-05-12	B0780101	–	–	1980-03-28	SWP 08582
					1990-10-12	SWP 39813
$\chi^1$ Ori	–	–	2000-03-10	o5bn02010	1990-02-01	SWP 38108
			2000-03-10	o5bn02020	1984-04-03	SWP 22408
$\kappa^1$ Cet	2000-09-10	A0830301	2000-09-19	o5bn03050	1994-09-14	SWP 52115
			2000-09-19	o5bn03060	1994-08-16	SWP 51829
					1994-08-16	SWP 51831
$\beta$ Com	2001-01-26	A0830401	–	–	1982-02-11	SWP 16313
					1979-08-14	SWP 06179
$\beta$ Hyi	2000-07-01	A0830101	–	–	1979-12-18	SWP 07430
					1979-12-03	SWP 07307
					1994-05-14	SWP 50765
					1992-03-13	SWP 44168

<sup>a</sup>EK Dra,  $\chi^1$  Ori,  $\kappa^1$  Cet, and  $\beta$  Hyi have ROSAT observations using the Boron filter but were not used here.

TABLE 4  
INTEGRATED FLUXES (IN UNITS OF ERG S<sup>-1</sup> CM<sup>-2</sup>) NORMALIZED TO A DISTANCE OF 1 AU AND TO THE RADIUS OF A ONE SOLAR MASS STAR. SEE TEXT FOR DETAILS

$\lambda$ interval (Å)	0.10 Gyr (EK Dra)	0.30 Gyr ( $\pi^1$ UMa + $\chi^1$ Ori)	0.65 Gyr ( $\kappa^1$ Cet)	1.6 Gyr ( $\beta$ Com)	4.56 Gyr (Sun)	6.7 Gyr ( $\beta$ Hyi)
[1–20]	180.2	21.5	7.76	0.976	0.15	0.048
[20–100]	82.4	14.8	10.7	2.80	0.70	0.321
[100–360]	187.2	69.4	22.7	(7.7)	2.05	(1.37)
[360–920]	((45.6))	((15.2))	((7.0))	((2.85))	1.00	((0.68))
[920–1180]	(18.1)	8.38	2.90	(1.70)	0.74	(0.50)
[1–360]+[920–1180]	467.9	114.1	44.1	13.2	3.64	2.2
[1–1180]	513.5	129.3	51.1	16.0	4.64	2.9

TABLE 5  
PARAMETERS OF THE POWER-LAW FITS TO THE MEASURED INTEGRATED FLUXES<sup>a</sup>

$\lambda$ interval (Å)	$\alpha$	$\beta$
[1–20]	2.40	-1.92
[20–100]	4.45	-1.27
[100–360]	13.5	-1.20
[360–920]	4.56	(-1.0)
[920–1180]	2.53	-0.85
[1–360]+[920–1180]	24.8	-1.27
[1–1180]	29.7	-1.23

<sup>a</sup>Relationship of the form: Flux =  $\alpha$  [age (Gyr)] $^{\beta}$ .

TABLE 6  
INTEGRATED FLUXES (IN UNITS OF ERG S<sup>-1</sup> CM<sup>-2</sup>) OF STRONG EMISSION FEATURES NORMALIZED TO A DISTANCE OF 1 AU  
AND THE RADIUS OF A ONE SOLAR MASS STAR. SEE TEXT FOR DETAILS

$\lambda$ (Å)	main elem.	0.10 Gyr (EK Dra)	0.30 Gyr ( $\pi^1$ UMa + $\chi^1$ Ori)	0.65 Gyr ( $\kappa^1$ Cet)	1.6 Gyr ( $\beta$ Com)	4.56 Gyr (Sun)	6.7 Gyr ( $\beta$ Hyi)
284	Fe XV	22.0	5.0	2.4	—	0.025	—
304	He II	44.3	8.3	2.3	—	0.260	—
335	Fe XVI	36.6	9.7	2.6	—	—	—
361	Fe XVI	15.7	6.6	1.6	—	0.016	—
584	He I	—	—	—	—	0.032	—
610&625	Mg X	—	—	—	—	0.028	—
630	O V	—	—	—	—	0.037	—
789	O IV	—	—	—	—	0.017	—
834	O II	—	—	—	—	0.015	—
977	C III	5.0	1.22	0.59	0.30	0.150	0.124
1026	H I	—	3.1	0.80	—	0.098	—
1032	O VI	3.1	0.75	0.43	0.16	0.050	0.048
1038	O VI	1.5	0.38	0.21	0.074	0.025	0.022
1176	C III	3.4	0.73	0.37	0.15	0.053	0.046
1206	Si III	—	1.12	0.75	—	0.095	—
1216	H I	—	42.2	29.3	—	6.19	—
1304	O I	4.3	1.18	0.60	0.45	0.143	0.163
1335	C II	4.7	1.52	0.95	0.36	0.188	0.155
1400	Si IV	4.3	1.59	0.77	0.28	0.083	0.097
1550	C IV	9.1	2.21	1.02	0.40	0.146	0.082
1640	He II	6.0	0.99	0.56	—	0.040	—
1657	C I	4.1	0.97	0.78	0.47	0.202	0.210

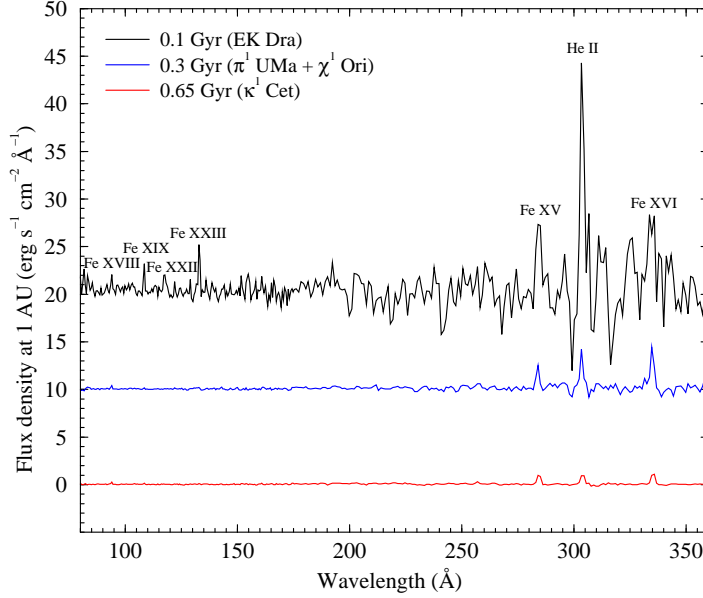


FIG. 2.—Extreme UV irradiances (flux density at 1 AU vs. wavelength) covering different stages of the evolution of solar-type stars. Some relevant features are identified. The spectra have been zeropoint-shifted using integer multiples of  $10 \text{ erg s}^{-1} \text{ cm}^{-2} \text{ Å}^{-1}$  to avoid confusion. Note the decrease in emission line strength from top to bottom (i.e., increasing age and rotation period).

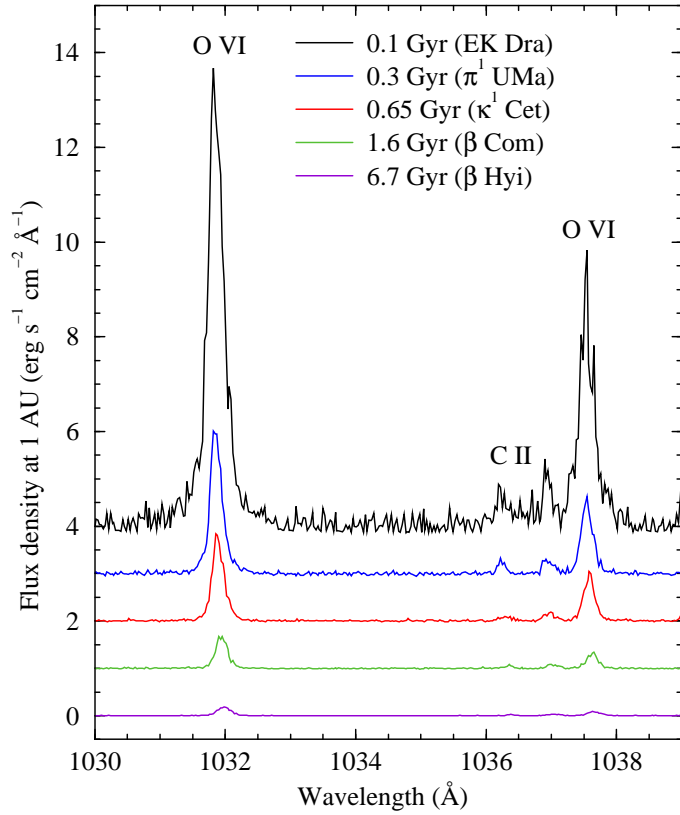


FIG. 3.—Details of the far-UV irradiances for different stages of the evolution of solar-type stars in the the region around the O VI  $\lambda\lambda 1032, 1038$  doublet. The spectra have been zeropoint-shifted using integer multiples of  $1 \text{ erg s}^{-1} \text{ cm}^{-2} \text{ Å}^{-1}$  to avoid confusion. Note the obvious trend of decreasing flux with increasing stellar age.

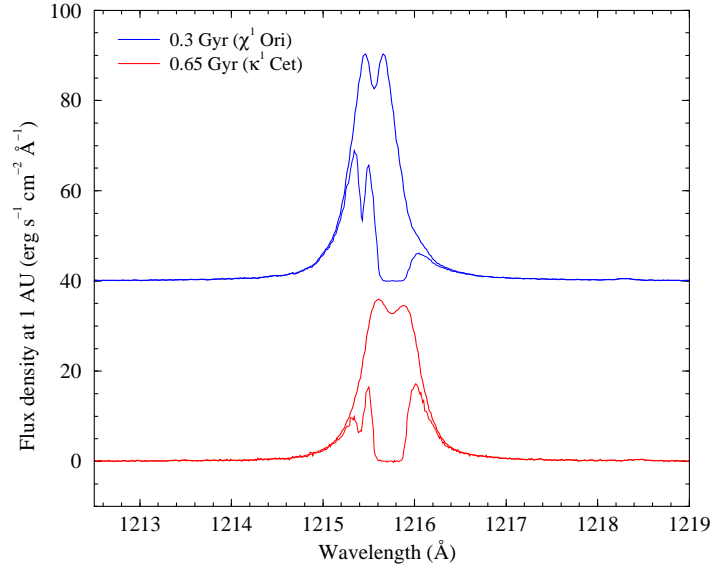


FIG. 4.— Detail of the H I Lyman $\alpha$  line of two solar-type stars of different ages. The thin lines show the observed profiles from HST spectra while the thick lines depict the reconstructed line profiles after correction for H I and D I ISM absorption. Irradiances are obtained by integrating the absorption-corrected profiles. The top spectrum has been shifted by  $40 \text{ erg s}^{-1} \text{ cm}^{-2} \text{ \AA}^{-1}$  to avoid confusion.

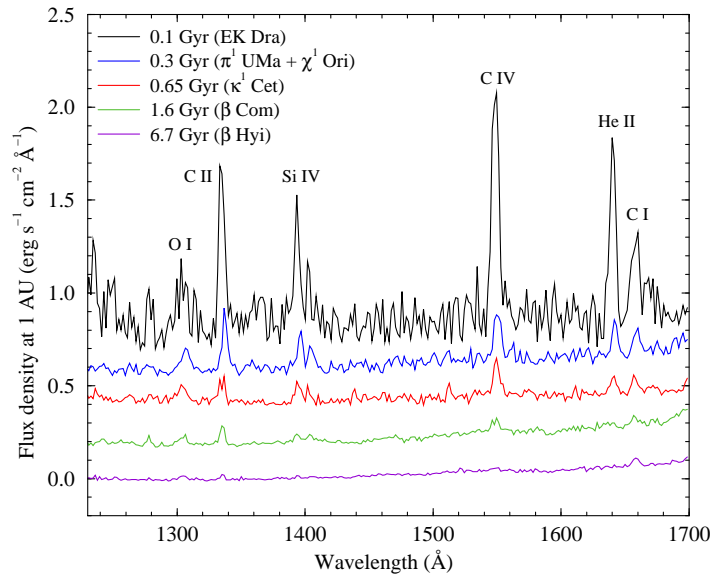


FIG. 5.— UV irradiances of solar-type stars at different stages of evolution. Some relevant features are identified. The emission line strength is found to decrease from top to bottom (i.e., increasing age and rotation period). The spectra have been zero-point-shifted using integer multiples of  $0.2 \text{ erg s}^{-1} \text{ cm}^{-2} \text{ \AA}^{-1}$  to avoid confusion. When compared with the EUVE and FUSE spectra, the emission lines seem broader here because of the lower spectral resolution of the observations. Note the onset of some weak photospheric (continuum) flux above 1500  $\text{\AA}$ .

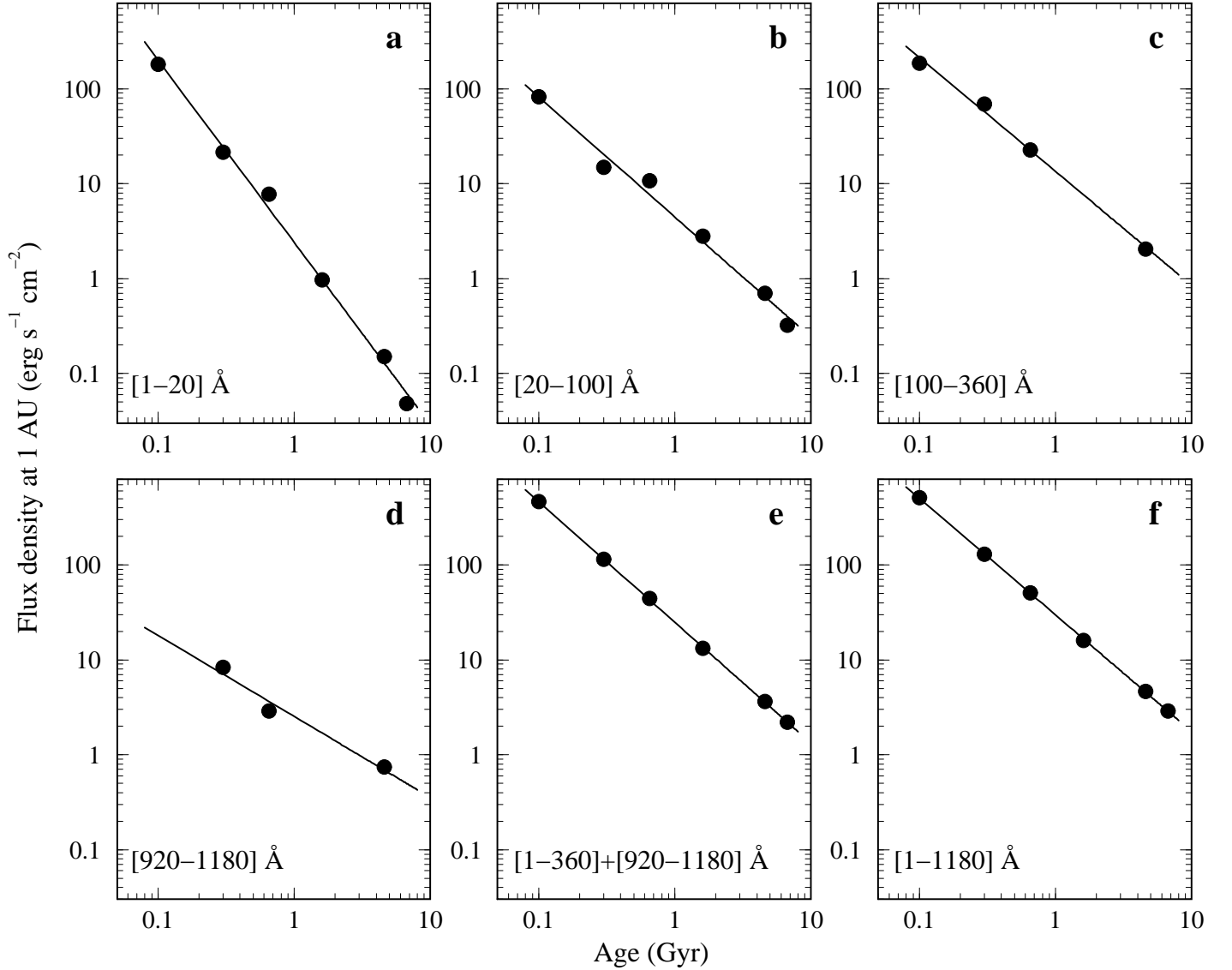


FIG. 6.— Power-law fits to the integrated irradiances in Table 4 for different wavelength intervals. The parameters of the resulting best-fitting relationships are given in Table 5.

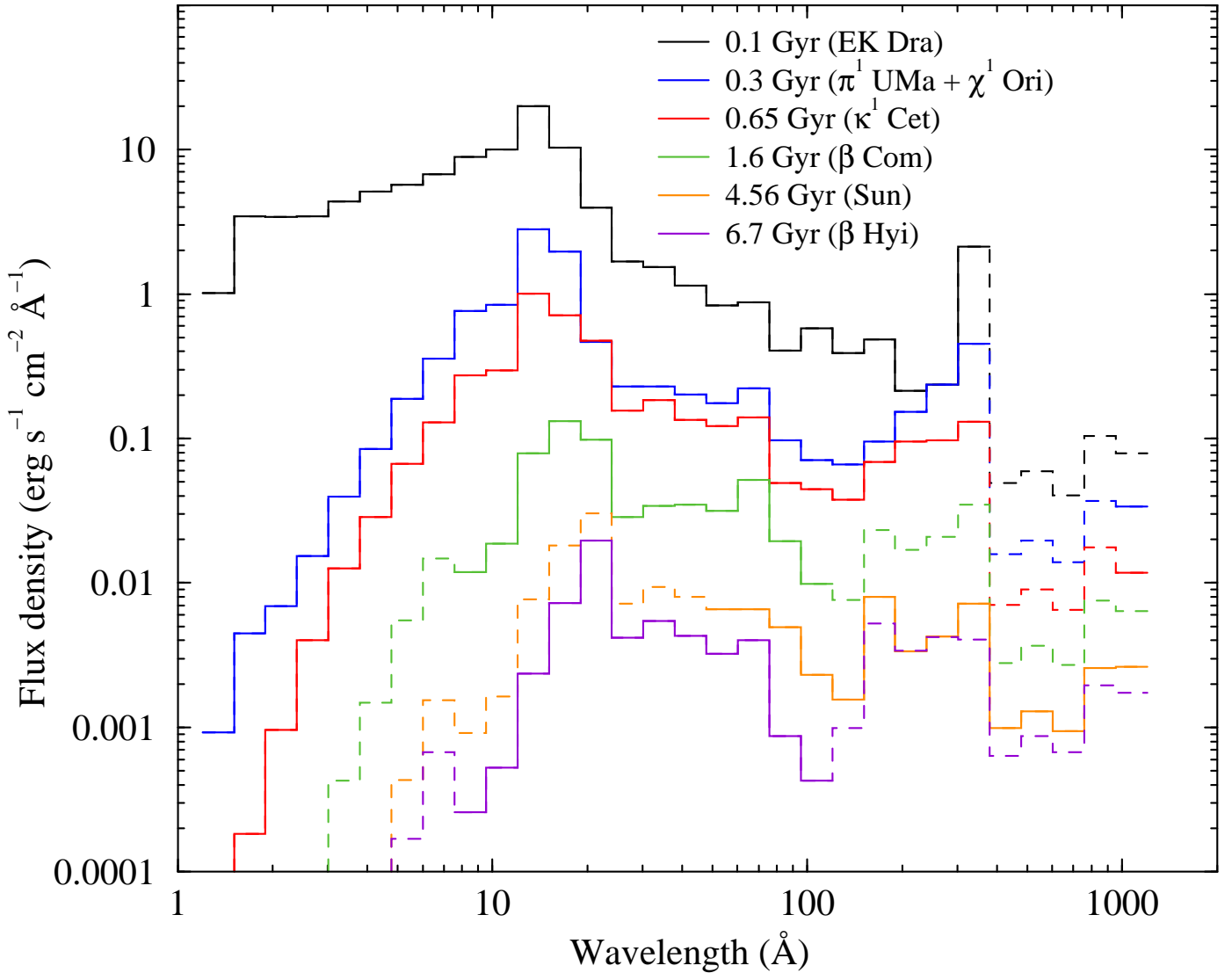


FIG. 7.— Full spectral energy distribution of the solar-type stars at different stages of the main sequence evolution. The solid lines represent measured fluxes while the dotted lines are fluxes calculated by interpolation using a power-law relationship.

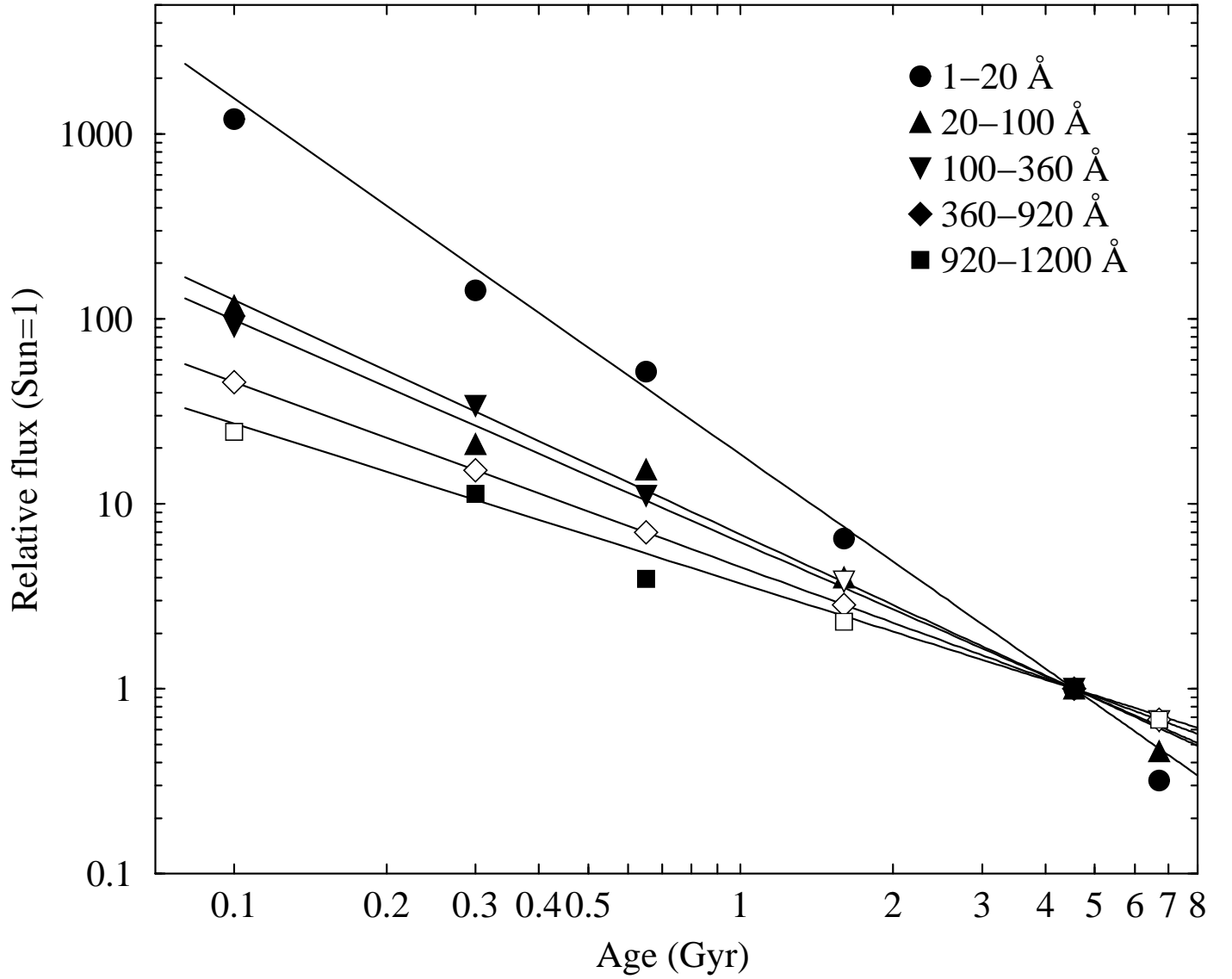


FIG. 8.— Solar-normalized fluxes vs. age for different stages of the evolution of solar-type stars. Plotted here are the measurements for different wavelength intervals (filled symbols) and the corresponding fits using power-law relationships with the slopes in Table 5. Represented with empty symbols are the inferred fluxes for those intervals with no available observations (values in parentheses in Table 4).

TABLE 7

ION FORMATION TEMPERATURES AND SLOPES OF THE POWER-LAW FITS TO THE MEASURED LINE FLUXES IN TABLE 6

$\lambda$ (Å)	main elem.	$\log T$	Slope
284	Fe XV	6.30	-1.79
304	He II	4.75	-1.34
335	Fe XVI	6.35	—
361	Fe XVI	6.35	-1.86
584	He I	4.25	—
610&625	Mg X	6.08	—
630	O V	5.26	—
789	O IV	5.05	—
834	O II	4.80	—
977	C III	4.68	-0.85
1026	H I	3.84	-1.24
1032	O VI	5.42	-1.00
1038	O VI	5.42	-1.02
1176	C III	4.68	-1.02
1206	Si III	4.40	-0.94
1216	H I	3.84	-0.72
1304	O I	3.85	-0.78
1335	C II	4.25	-0.78
1400	Si IV	4.75	-0.97
1550	C IV	5.00	-1.08
1640	He II	4.75	-1.28
1657	C I	3.85	-0.68